Applied Surface Science Advances 7 (2022) 100200

Contents lists available at ScienceDirect

Applied Surface Science Advances

journal homepage: www.sciencedirect.com/journal/applied-surface-science-advances

Corrosion behaviour of new oxo-pyrimidine derivatives on mild steel in acidic media: Experimental, surface characterization, theoretical, and Monte Carlo studies

Khaled Saad Miled Ferigita [a], Mothana Ghazi Kadhim AlFalah [a,b,*], Murat Saracoglu [c], Zülbiye Kokbudak [d], Savaş Kaya [e], Muna Omar Abdels Alaghani [f], Fatma Kandemirli [g]

[a] Metallurgy and Materials Engineering Department, Faculty of Engineering and Architecture, Kastamonu University, Kastamonu 37150, Turkey
[b] Materials of Engineering Department, College of Engineering, University of Al–Qadisiyah, Al–Qadisiyah 58002, Iraq
[c] Erciyes University, Faculty of Education, Kayseri 38039, Turkey
[d] Erciyes University, Faculty of Science, Department of Chemistry, Kayseri, Turkey
[e] Sivas Cumhuriyet University, Health Services Vocational School, Department of Pharmacy, Sivas 58140, Turkey
[f] University of Benghazi, Faculty Engineering, Benghazi, Libya
[g] Biomedical Engineering Department, Faculty of Engineering and Architecture, Kastamonu University, Kastamonu 37150, Turkey

ARTICLE INFO

Keywords:
Mild steel
Oxo-pyrimidine
Corrosion resistance
EIS
Monte Carlo

ABSTRACT

In this work, the effects of new compounds, namely, 1-amino-5-(4-methylbenzoyl)-4-(4-methylphenyl) pyrimidin-2 (1*H*)-thione (AMMP), and 1-(5-(4-Methoxybenzoyl)-4-(4-methoxyphenyl) 2-oxopyrimidin-1 (2*H*)-yl)-3-phenylthiourea (MMOPH) has been successfully investigated as a corrosion inhibitor for mild steel in a 1 M HCl solution. This investigation has been done by electrochemical techniques (potentiodynamic polarization, and electrochemical impedance spectroscopy), surface characterization (scanning electron microscopy with energy dispersive x-ray spectroscopy, and atomic force microscopy), and theoretical calculations (density function theory and Monte Carlo simulation). The electrochemical results showed that both compounds act as mixed-type inhibitors. However, MMOPH is more efficient than AMMP (95.9% compared with 84.1% at 5×10^{-4} M and an immersion time of 1 h). Additionally, the effect of immersion time on inhibitor efficiency was studied. The current density was reduced with the presence of inhibitors from 517.93 to 56.18 and 9.96 $\mu A.cm^{-2}$ at 5×10^{-4} M and an immersion time of 1 h for AMMP and MMOPH, respectively. In both substances, the Langmuir isotherm system showed the best fit, with physisorption and chemisorption being the types of adsorption. The results of surface characterization indicated that both compounds can be adsorbed on mild steel surfaces to minimize corrosion. The obtained Monte Carlo simulation results suggest that the inhibitors are adsorbed vertically and the formation of a protective layer on the metal surface. The density function theory calculations for inhibitors found the protonated state is more reactive than the neutral state and agree with experimental results and follow the order MMOPH > AMMP. The results showed that both compounds can be used as new corrosion inhibitors for mild steel in aggressive environments.

1. Introduction

Corrosion related technology and industrial failures cannot be allowed in a contemporary firm, particularly where human injuries, deaths, unexpected shutdowns, and environmental contamination are involved. Thus, corrosion management both during the design phase and during operation is a need for the modern period [1–5]. Mild steel is a metal that is used in practically every sector in the world at every step of production, most notably in the oil sector, due to its unmatched mechanical qualities and economic viability [6–11]. One of the primary issues with mild steel is its corrosion in sectors that produce oil and in several transportation networks, which results in increased damage. The solutions, HCl and H_2SO_4, are employed in a variety of industrial procedures to remove undesirable hard scales and rust, as well as in acid pickling and oil well cleaning. Iron and its alloys such as mild steel corrode significantly in the presence of strong acid, causing serious

* Corresponding author.
E-mail addresses: mothana.kadhim@qu.edu.iq, muthanakadhem@yahoo.com (M.G.K. AlFalah).

https://doi.org/10.1016/j.apsadv.2021.100200
Received 7 September 2021; Received in revised form 14 November 2021; Accepted 14 December 2021
Available online 26 December 2021

damage to the pipe walls and eventually resulting in the breakdown of the petroleum pipeline, resulting in increased environmental pollution and financial loss [12]. Let us stay in the same industrial context: the selection of acidic solutions is a top priority due to their high effectiveness in specific industrial applications. Between several acids, the most often employed is hydrochloric acid solution, which is used as a stripping or cleaning agent. It is also frequently used in the stimulation of oil wells and in the removal of localized deposits. The corrosive nature of hydrochloric acid necessitates the use of corrosion inhibitors, which are necessary to limit the damage to metallurgical materials [13]. Nowadays, amongst other practical ways such as cathodic and anodic protection, alloying, and coating, the use of inhibitors has been demonstrated to be the most effective approach for protecting metals from acid corrosion [14–18]. Corrosion prevention approaches using inhibitors have gained popularity due to their suitability, efficiency, and economic feasibility. According to a review of the literature, organic molecules protect metal surfaces against corrosion by adsorbing on them. Heterocyclic organic molecules with - electrons and functional groups comprising S, O, and N are the most effective corrosion inhibitors. This behaviour might be caused by the interaction of metals with the heteroatoms and pi-electrons of organic inhibitors [19–22]. Additionally, the synthesis inhibitor requires an electron cloud on the aromatic ring as well as a C = N group, both of which are predicted to provide more adsorption surface area on the steel, hence producing a more efficient inhibition. Furthermore, in hydrochloric acid, nitrogen-containing organic inhibitors are effective anticorrosion materials for metals, while sulfur-containing compounds are effective inhibitors. For both mediums, nitrogen and sulfur-containing compounds act as excellent corrosion inhibitors [10,23–25]. A compound that helps prevent corrosion is adsorbed depending on its structure, metal surface characteristics, and solution composition [26–30]. Because of the toxicity, expense, and environmental problems associated with many of the organic inhibitors documented in the literature, it is crucial to find non-toxic, affordable, and environmentally acceptable inhibitors. Pyrimidine compounds have been shown to be environmentally beneficial corrosion inhibitors [31]. Pyrimidine derivatives are a class of nitrogen heterocycles that are often employed in medicine [32–35]. Many biological activities such as antibacterial, anticonvulsive, antifungal, antiviral, antidiabetic, and anticancer characteristics are found in these substances [36–38].

Numerous chemical compounds containing the pyrimidine group have been explored for their corrosion inhibitory properties in a variety of corrosive solutions [39–43]. Yadav et al. [44] investigated new pyrimidine derivatives, namely, 7-methoxypyrido [2,3-d] pyrimidin-4-amine (MPPA) and 4-amino-7- methoxypyrido[2,3-*d*]pyrimidin-2(1H)-one (AMPO) as corrosion inhibitors for mild steel in 15% HCl. They used electrochemical methods (such as potentiodynamic polarization and electrochemical impedance spectroscopy (EIS)), surface characterization (SEM, EDX, and AFM), and density function theory (DFT) to evaluate the efficacy of these inhibitors. Their results showed that the inhibitor efficiency of MPPA was higher than of AMPO (97.8% compared to 96.9% at 200 ppm). Haque et al. [45] presented two pyrimidine derivatives, namely 5-styryl-2,7-dithioxo- 2,3,5,6,7,8-hexahydropyrimido[4,5-d] pyrimidin-4(1H) one (PP-1) and 5-(2-hydroxyphenyl)−2,7- dithioxo-2,3,5,6,7,8-hexahydropyrimido[4,5-*d*]-pyrimidin-4(1H) one (PP-2) as corrosion inhibitor for N80 steel in 15% HCl. They utilized experimental and theoretical methods to determine the corrosion inhibitor efficiency. Based on the obtained theoretical results, the order of inhibition was PP-1 > PP-2 (IE= 87% compared to IE=73.9%). Nadia Arrousse et al. [20] introduced two compounds, namely, 2-(((1H-pyrazol-1-yl) methyl) amino) pyrimidine-4,6- diol (DPP) and 2-(bis((1H-pyrazol-1-yl) methyl) amino) pyrimidine-4,6- diol (PP) as a good corrosion inhibitor for mild steel in 15% HCl. They used multiples of experimental and theoretical methods to calculate corrosion inhibitor efficiency. They found that the current density reduction was due to electron-rich molecules adsorbing on the mild steel surface. Their results showed that the inhibitor efficiency of PP (IE=91%) was higher than of DPP (81%). Also, the electrochemical results indicated that both compounds appeared to be mixed types with predominant anodic.

Our AMMP and MMOPH molecules are synthetic substances that include amino, pyrimidine, thiourea, or oxo-pyrimidin. Due to the presence of sufficient nitrogen, sulfur, oxygen, and delocalized π-electrons in these compounds (AMMP and MMOPH), it is predicted that they would exhibit a high corrosion prevention effectiveness. Pyrimidine compounds have also been shown to be effective mild steel MS inhibitors in acid solutions [26].

According to reasons mentioned above and based on the literature and in a way to try to mitigate the expensive costs due to corrosion problems in the industries, we have chosen two newly pyrimidine derivatives, namely, "1-amino-5-(4-methylbenzoyl)−4-(4-methylphenyl) pyrimidin-2 (1*H*)-thione (AMMP), and 1-(5-(4-Methoxybenzoyl)−4-(4-methoxyphenyl)−2-oxopyrimidin-1(2*H*)-yl)−3-phenylthiourea (MMOPH)" [48] as corrosion inhibitor for mild steel in 1 M HCl. Synthesis and characterization of these compounds have been reported in our reference [46]. Electrochemical techniques including linear polarization resistance, potentiodynamic polarization, and electrochemical impedance spectroscopy have been used to determine corrosion performance. SEM, EDX, and AFM studies were all used to examine the surface of the inhibited sample. The electronic and molecular structures of substituted pyrimidine derivatives were studied theoretically using density function theory (DFT) and Monte Carlo simulations (MCS) in order to determine which of them is the most efficient corrosion inhibitor.

2. Experimental

2.1. Preparation of samples

The MS bar was bought from a local market with a chemical composition (wt.%) of 0.18% C, 0.0556% Cr, 1.018% Si, 0.699% Mn, 0.0939% Cu, 0.0853% Ni, and 97.87% Fe. In order to prepare the sample for working electrode, mild steel was cut into a cylindrical shape with dimensions (0.8 cm in diameter and 3 cm in length). Copper wire was used to link the substrates from the back before immersing them in an epoxy resin with a naked area left without covering 0.502 cm^2. Silicon carbide was used to polish the samples, with settings ranging from 600 to 2400. After that, the sample was washed with acetone, water which had been purified twice, and then left to dry at room temperature. The chemical compounds "1-amino-5-(4-methylbenzoyl)−4-(4-methylphenyl) pyrimidin-2 (1*H*)-thione (AMMP), and 1-(5-(4-Methoxybenzoyl)−4-(4-methoxyphenyl)−2-oxopyrimidin-1(2*H*)-yl)−3-phenylthiourea" (MMOPH) were synthesised, characterized, and published by our colleagues (see Figure 1) [46].

2.2. Preparation of solution cell

The research solutions were produced using 37% HCl (Sigma-Aldrich, USA), AMMP, or MMOPH. The inhibitor solution with the maximum concentration (5×10^{-4} M) was made by dissolving the desired quantity of AMMP or MMOPH in 1 M HCl. The inhibitor media was generated at lower concentrations (1×10^{-5} M, 5×10^{-5} M, and 1×10^{-4} M) using the dilution procedure. The compounds were completely soluble in 1 M HCl solution.

2.3. Electrochemical tests

For electrochemical testing of the corrosion behaviour of mild steel, a potentiostat equipped with the necessary software (Ivium Technologies' CompactStat Electrochemical Interface, Instrument: B08024, Software: 2699(699)) was utilized. Platinum wire, Ag/AgCl, and mild steel were used as the counter electrode, reference electrode, and working

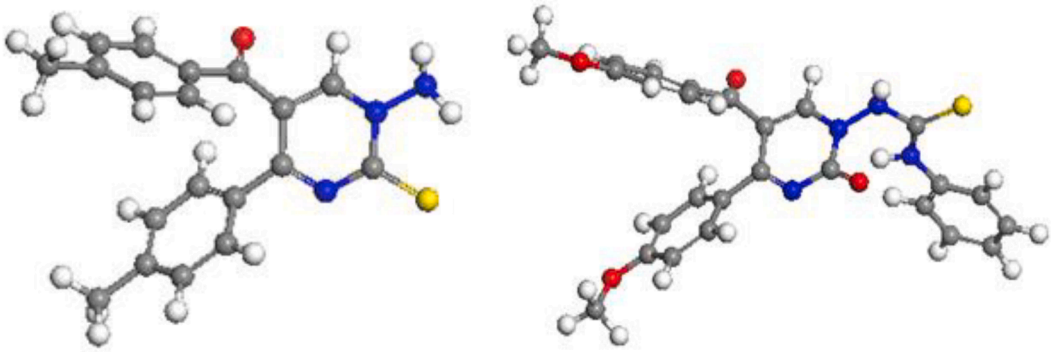

1-Amino-5-(4-methylbenzoyl)-4-(4-methylphenyl) pyrimidin-2 (1H)-thione (AMMP)

1-(5-(4-Methoxybenzoyl)-4-(4-methoxyphenyl)-2-oxopyrimidin-1(2H)-yl)-3-phenylthiourea (MMOPH)

Fig. 1. Molecular structure of investigated compounds AMMP and MMOPH.

electrode respectively. The acidic solution utilized in this study was a 1 M HCl solution. This study used both alternating current electrochemical methods such as impedance spectroscopy (EIS) and direct current electrochemical techniques such as potentiodynamic polarization and linear polarization resistance. To establish a stable surface state, the samples were immersed for one hour at ambient temperature (298 K) in a 1 M HCl stagnant solution. The working electrode was submerged in the test solution for 1 hour before beginning the electrochemical impedance spectroscopy (EIS), linear polarization resistance (LPR), and potentiodynamic polarization (PDP) to achieve a relatively steady state and to create open circuit potential (OCP). The EIS values were determined throughout a frequency range of 100 kHz to 10 mHz with an amplitude of 5 mV. In this instance, measurements of the LPR (along with its variation, the voltage shift of LPR) were conducted at ± 10 mV of open circuit potential (OCP) at 60 mV/min scan rate, while measurements of the potentiodynamic polarization (PDP) were carried out at a scan rate of 60 mV/min with −0.250 V as related to OCP towards cathodic curve and +0.250 V as related to OCP towards anodic curve. Additionally, because it is not a destructive method, AC measurement is the best technique for extending immersion time without disturbing the solution cell. Therefore, the electrochemical impedance spectroscopy was carried out at 24 h and 72 h. All electrochemical studies on each compound were done at least three times to verify repeatability. All curves in this work have been matched to a surface area of 1 cm^2.

2.4. Surface characterization

SEM-EDX and AFM spectroscopic investigation of the surface. After a 72-hour immersion time at room temperature in acidic conditions, the samples are removed from the test solutions and dried. SEM micrographs were obtained in high vacuum mode using a (FEI-Quanta, Hillsboro, OR, USA) FEG 250 SEM, accelerating voltage (HV) =15 KV. AFM measurements were made using a Bruker EDGE 3-SYS AFM. Au/Pd (60%−40%) coating was applied to the surface in order to obtain high resolution images from SEM measurements and to perform EDX analysis under high voltage. In addition, because the oxide layer formed on the surface of metal samples forms during measurement and prevents measurement, samples are coated. The coating was applied under 40 mA current for 30 s by utilizing the Quanta FEG 250 model of the FEI brand. The AFM measurement settings were as follows: peak force taping mode, which is an intermittent contact mode; and 3 × 3 μm^2 scan area. Additionally, EDX analysis was used in combination with SEM to assess the weight% composition of the mild steel samples.

2.4.1. Density functional theory studies (DFT)

To confirm the electrochemical results, DFT studies were conducted using the DMol3 module in Material Studio 2017 (Method: GGA/BLYP; Basis set: DNP 3.5; Solvation model: COSMO). The protonated form of the quantum chemical of AMMP and MMOPH molecules was determined by using Gaussian 09 software at B3LYP-6–311 in the water phase at 298 K. Numerous DFT indices have been computed using the following relationships from the energies of frontier molecular orbitals (E_{HOMO} and E_{LUMO}) and listed in Table. 6 [47–49]:

$$I = -E_{HOMO} \tag{1}$$

$$A = -E_{LUMO} \tag{2}$$

$$\chi = \frac{I + A}{2} \tag{3}$$

$$\eta = \frac{I - A}{2} \tag{4}$$

$$\mu = -\chi \tag{5}$$

$$\Delta E = E_{LUMO} - E_{HOMO} \tag{6}$$

$$\Delta N = \frac{(\chi_{Fe} - \chi_{inh})}{2(\eta_{Fe} + \eta_{inh})} \tag{7}$$

In the previous equations (Eqs. (1)–(7)), E_{HOMO} and E_{LUMO} indicate the energy of the highest occupied molecular orbital and the lowest occupied molecular orbital, respectively, in the occupied molecular orbital system. I and A refer to the ionization potential and the electron affinity, respectively. Where χ, η, μ, ΔE, and ΔN refer to electronegativity, chemical potential, hardness, energy band, and electron transfer fraction, respectively. It was necessary to use the work function of Fe ($\chi_{Fe} = 7$ eV) and η_{Fe} ($\eta_{Fe} = 0$) to get the value of ΔN.

2.4.2. Monte Carlo simulations (MCS)

The interaction between the adsorbate and substrate compounds was underlined via the use of Monte Carlo (MCS) simulations offered by Material Studio (2017)'s adsorption locator module. The Adsorption Locator module was used by BIOVIA Company to develop a system using the Monte Carlo (MC) simulation approach. Studying the interfacial contacts between the steel surface and the inhibitor molecules using Monte Carlo simulations is an intriguing approach that may give us additional knowledge about these interactions. The time step (1fs) and simulation time (100 ps) during the simulation were used to conduct MC simulations in conjunction with a simulated annealing method. Pregeometrized conformers were created and administered at a temperature of 298 K using Berendsen's thermostat. In order to get findings of high quality, the convergence thresholds for displacement, force, and energy were set at 0.015 Å, 0.5 $kcal.mol^{-1}$. Å, and 10^{-3} $kcal.mol^{-1}$, respectively. The system included a 150 H_2O + $3H_3O^+$ + $3Cl^-$ + 1 inhibitor, while the simulation box dimensions were: 24.82 Å × 24.82 Å ×

94.19 Å (8 layers of Fe (110), 80 Å as a vacuum region, and super cell: 10 × 10). We selected the Fe (110) surface to model the adsorption process because of the high density of the packed surface and the high degree of stability it exhibited throughout the simulation. The bulk atoms on the Fe (1 1 0) plane were kept frozen. In order to calculate the electrostatic potential energy, the Ewald summation technique was utilized, while the atom-based methodology was used to calculate the van der Waals potential energy. For the purpose of optimizing the structures of all components of the system under consideration, the force field COMPASS was used [50–52]. The geometry optimization stage has been done by the Forcite module.

Eqs. (8) and 9 were used to determine the adsorption energy and binding energy of the examined AMMP and MMOPH on the Fe substrate and recorded in Table 7 [51].

$$E_{ads} = E_{total} - E_{Metal\ surface} - E_{Inhibitor} \quad (8)$$

$$E_{ads} = -E_{Binding} \quad (9)$$

Where E_{total}, $E_{Metal\ surface}$, and $E_{Inhibitor}$ refers to the total energy of the system, energy of the metal surface, and energy of the inhibitor respectively.

3. Results and discussion

3.1. Electrochemical investigations

3.1.1. OCP, PDP and LPR testes

The working electrode's potential in relation to the reference electrode when no external current is applied is referred to as the open circuit potential. Its measurement is needed to determine the period of immersion time required to produce steady state conditions, which are required before conducting electrochemical experiments.Fig. 2 (A-B) shows open circuit potential (OCP) vs. time curves for uninhibited and inhibited mild steel with the presence of inhibitors AMMP and MMOPH, respectively at immersion time 1 h and 25 °C. Fig. 2 (A-B) shows that the OCP of the uninhibited MS submerged in the initial acid solution gradually decreases (started at −0.427 V with non-linear behaviour) due to metal dissolution, followed by a quasi-steady state at roughly 60 min of immersion time (steady state was arrived at a value of −0.437 V) due to iron oxide and hydroxide production. When a mild steel was inhibited in the presence of the inhibitor AMMP (Fig. 2(A)) at concentrations of 1 × 10^{-5}, 5 × 10^{-5}, and 1 × 10^{-4} M, the OCP was first set to −0.353, −0.352, and −0.320 V, respectively, and then gradually reduced to a more negative value. After an hour, it stabilized at −0.378, −0.353, and −0.346 V respectively. However, the OCP curve at high concentration (5 × 10^{-4} M) started at a value of −0.432 V and increased sharply towards more positive with a value of −0.425 V at the beginning of immersion, and then it steadily decreased to more negative until it gained a steady state at the end of immersion with a value of −0.464 V. This might be related to the initiation of aggressive ion diffusion into the oxide layer, such as hydrogen and chloride. Additionally, parallel OCP vs. time curves were seen owing to the elimination of the accumulated oxide layer on the surface of mild steel by adsorption of AMMP molecules. Similar behaviour was observed in the case of inhibited mild steel by inhibitor MMOPH (Fig.2(B)) at concentrations of 1 × 10^{-5}, 5 × 10^{-5}, 1 × 10^{-4}, and 5 × 10^{-4} M. The OCP started with −0.383, −0.376,−0.367, and −0.367 V respectively. After some time, the OCP decreased steadily to more negative value until it approached a stable state with values of −0.429, −0.412, −0.400, and −0.381 V after one hour, respectively. This behaviour implies the creation of a protective layer on the metal surface as a result of the inhibitor molecules' adsorption, hence reducing the active sites on the MS surface. M.A. Migahed et al. [53] and M.G.K. AlFalah et al. [54] described this behaviour. The high positive OCP values are related to the productive action of AMMP and MMOPH composites in blocking violent ions such as hydrogen and chloride from adhering to the metal's surface [54].

It's possible to extract certain critical parameters of the corrosion process, as well as the type of inhibitors used, whether anodic, cathodic, or a mix of both, using potentiodynamic polarization while the inhibitors are added. The PDP exams were conducted for an hour in this research. All data, including inhibitor effectiveness IE%, surface coverage (θ),i_{corr} ∘, E_{Corr}, β_a, β_c, and R_{LPR} were collected using PDP and LPR methods and are summarized in Table 1.

Corrosion current density = i_{corr} ∘
Corrosion potential = E_{Corr}
Anodic Tafel slopes = β_a
Cathodic Tafel slopes = β_c
Polarization resistance = R_{LPR}

The following equations were used to calculate the inhibitor efficiency [55,56]:

$$IE_{PDP}\ (\%) = \frac{i_{corr\ -\circ} i_{corr(inh)}}{i_{corr\circ}} \times 100 \quad (10)$$

Where i_{corr} ∘ and $i_{corr(inh)}$denote uninhibited and inhibited mild steel current densities, respectively.

$$IE_{LPR}\ (\%) = \frac{R_{P\ (inh)} - R_{P\circ}}{R_{P\ (inh)}} \times 100 \quad (11)$$

Where $R_{P\circ}$ and $R_{P\ (inh)}$ denote the polarization resistance of mild steel in its uninhibited and inhibited states, respectively.

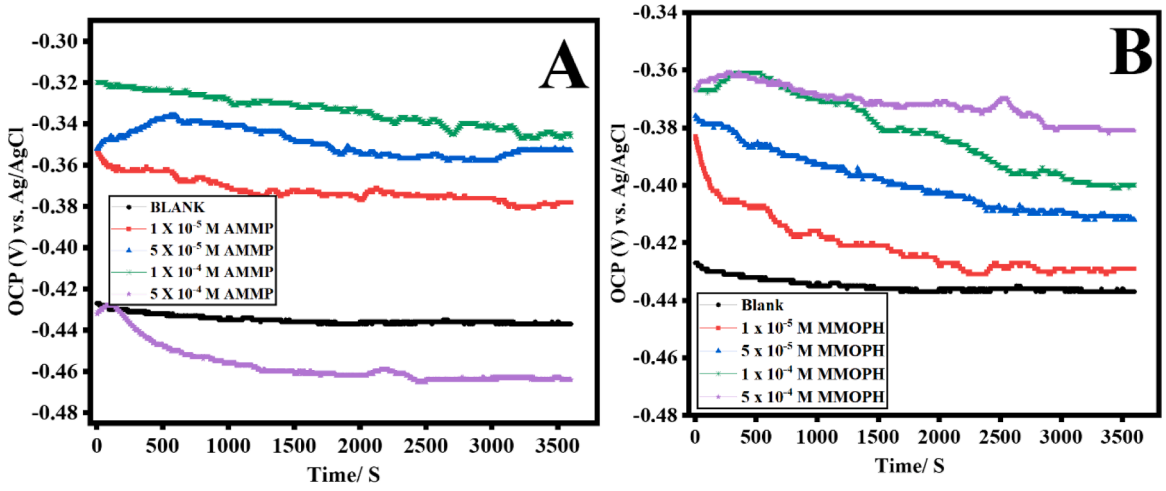

Fig. 2. OCP for mild steel without and with the presence of inhibitors, AMMP (A) and MMOPH (B), 1 h at 298 K.

Table 1
Potentiodynamic Polarization and Linear Polarization Resistance for mild steel immersion in 1 M HCl at 298 K without and with the presence of corrosion inhibitors AMMP and MMOPH at 1 h.

Time	Concentration (M)	E_{corr} (V)	i_{corr} ($\mu A.cm^{-2}$)	$-\beta_c$ (V/dec)	β_α (V/dec)	θ	% IE	R_{lp} ($\Omega.cm^2$)	θ	% IE
	BLANK	−0.4784 ± 0.001	517.93 ± 0.2	0.127 ± 0.003	0.105 ± 0.004	——	——	55.57 ± 1	——	——
AMMP1 h	1×10^{-5}	−0.4816 ± 0.001	316.73 ± 0.1	0.128 ± 0.002	0.100 ± 0.002	0.3884	38.84	78.41 ± 2	0.2912	29.12
	5×10^{-5}	−0.4803 ± 0.002	221.12 ± 0.2	0.139 ± 0.006	0.113 ± 0.001	0.573	57.3	113.85 ± 2	0.5119	51.19
	1×10^{-4}	−0.4790 ± 0.001	105.97 ± 0.3	0.112 ± 0.008	0.084 ± 0.006	0.7953	79.53	179.06 ± 3	0.6896	68.96
	5×10^{-4}	−0.4938±0.001	56.18 ± 0.4	0.105 ± 0.007	0.111 ± 0.004	0.8915	89.15	363.50 ± 4	0.8471	84.71
	BLANK	−0.4784 ± 0.002	517.93 ± 0.3	0.127 ± 0.003	0.105 ± 0.004	——	——	55.57 ± 1	——	——
MMOPH1 h	1×10^{-5}	−0.4453 ± 0.003	43.42 ± 0.2	0.117 ± 0.004	0.079 ± 0.001	0.9162	91.62	499.29 ± 2	0.8887	88.87
	5×10^{-5}	−0.4549 ± 0.002	37.08 ± 0.3	0.101 ± 0.002	0.077 ± 0.004	0.9284	92.84	527.13 ± 4	0.8946	89.46
	1×10^{-4}	−0.4468 ± 0.003	27.34 ± 0.4	0.109 ± 0.003	0.074 ± 0.003	0.9472	94.72	668.16 ± 4	0.9168	91.68
	5×10^{-4}	−0.4384 ± 0.002	9.96 ± 0.3	0.096 ± 0.006	0.056 ± 0.002	0.9808	98.08	1503.49 ± 6	0.963	96.3

In 1 M HCl at 1 h, the PDP curves for uninhibited mild steel and MS that has been inhibited with different doses of AMMP and MMOPH, respectively, are shown in Figs. 3 and 4. In Fig. 3, it can be observed that the inhibitor has an effect on the anodic and cathodic curves, with the cathodic reaction being the most adversely impacted. The fact that current densities decrease significantly (from 517.93 to 56.18 $\mu A.cm^{-2}$) with increasing concentrations of the AMMP indicates that the inhibitive action is caused by adsorption of the AMMP on the electrodes. This is similar observed in H. Keles¸ et al. [19]. Furthermore, with the addition of inhibitors, the Tafel slope (β_c) was somewhat deviated, which refers to the inhibitive activity of the cathodic sites on a steel surface caused by basic blockage and results in a reduction in hydrogen evolution (Tables. 1). Likewise, with the addition of the inhibitors, the values of anodic Tafel slopes (β_a) (Tables. 1) fluctuate somewhat, showing that these molecules are first adsorbed to the mild steel surface and then inhibited by simply blocking the metal surface reaction sites. In other words, the Tafel slopes values show that inhibitors had no effect on the corrosion mechanism. The inhibitory effect of the tested substances is achieved by the inhibitor's molecule adsorbing on the electrode surface and blocking the active sites [57]. It can be seen clear from Fig. 4 that the performance of the MMOPH was more efficient than the AMMP. The current density decreased sharply (from 517.93 to 9.96 $\mu A.cm^{-2}$) with increasing concentration of the MMOPH. An insoluble iron-inhibitor complex may be formed by the binding of nitrogen atoms of a pyrimidine compound carrying a pair of electrons to an iron sample in solution. As a result of the complicated interactions between the test compound and the steel surface, the inhibitory effect of this organic molecule is confirmed. As a consequence of the changes in obstacles of an excess of energy of both

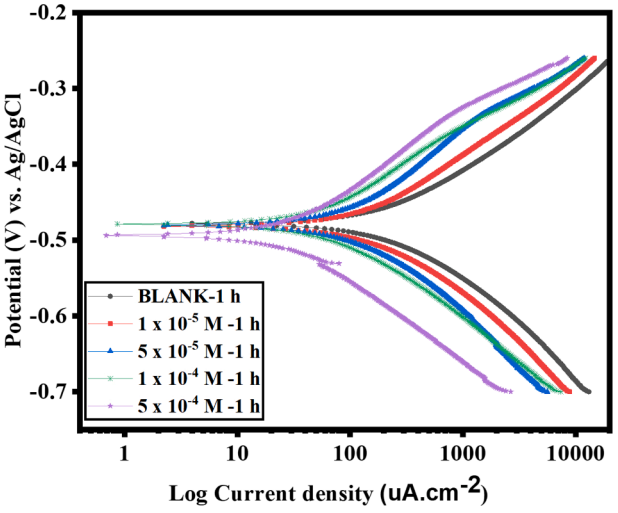

Fig. 3. Potentiodynamic polarization (PDP) for uninhibited mild steel and inhibited with the presence of inhibitor AMMP with different concentration at immersion time 1 h in 1 M HCl at 298 K.

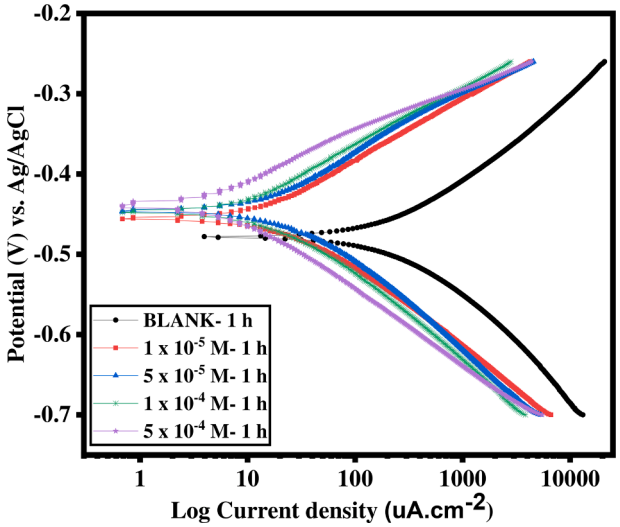

Fig. 4. Potentiodynamic polarization (PDP) for uninhibited mild steel and inhibited with the presence of inhibitor MMOPH with different concentration at immersion time 1 h in 1 M HCl at 298 K.

electrochemical processes that take place throughout this phase, the inhibitory effects arise [58].

In terms of the shift in corrosion potentials, the AMMP causes the corrosion potential to move more negatively towards the cathodic zone, whereas the MMOPH causes the corrosion potential to shift less negatively towards the anodic region (see Figs. 3 and 4, and Table 1). It is hypothesized that the rivalry between the suppression of cathodic and anodic processes has an impact on corrosion's potential value [59]. Previous research has shown that if the corrosion potential values of these displacements are higher than −0.085 V, inhibitors may be classified as cathodic or anodic, and if the displacements are less than −0.085 V, inhibitors can be classified as mixed [60]. According to results shown in Table 1, both compounds exhibited corrosion potential less than −0.085 V. As a result, both substances functioned as corrosion inhibitors of a mixed type.

In contrast, the LPR findings in Table 1 show that LPR follows an order of MMOPH (IE=96.30%) > AMMP (IE=84.71%), which is incompatible with i_{corr}∘. This means that the i_{corr} ∘ and the $1/R_{LPR}$ values are proportionate [61].

3.1.2. *Impedance tests*

It's possible to get useful kinetic information on the metal/solution interaction by using EIS measuring technology. Figs. 5 and 6 (A-C) show the Nyquist and Bode curves of uninhibited MS and inhibited in 1 M HCl at immersion time of 1 h for the AMMP and MMOPH respectively. At 1 h immersion time, the Nyquist spectra of the uninhibited solution revealed a single semi-circular capacitive loop. This indicates that mild steel

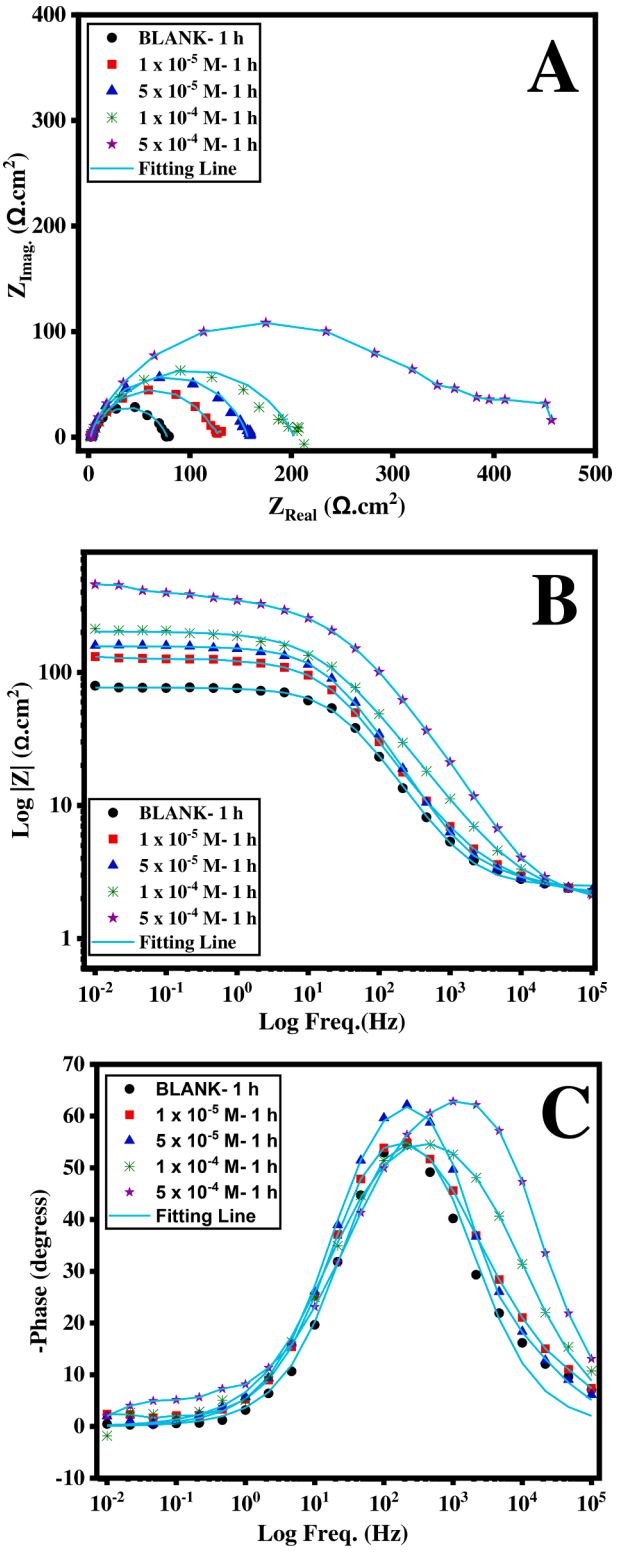

Fig. 5. Impedance spectroscopy (EIS) for uninhibited mild steel and inhibited with the presence of inhibitor AMMP with different concentration at immersion time 1 h in 1 M HCl at 298 K, Nyquist curve (A), Bode curves (B-C).

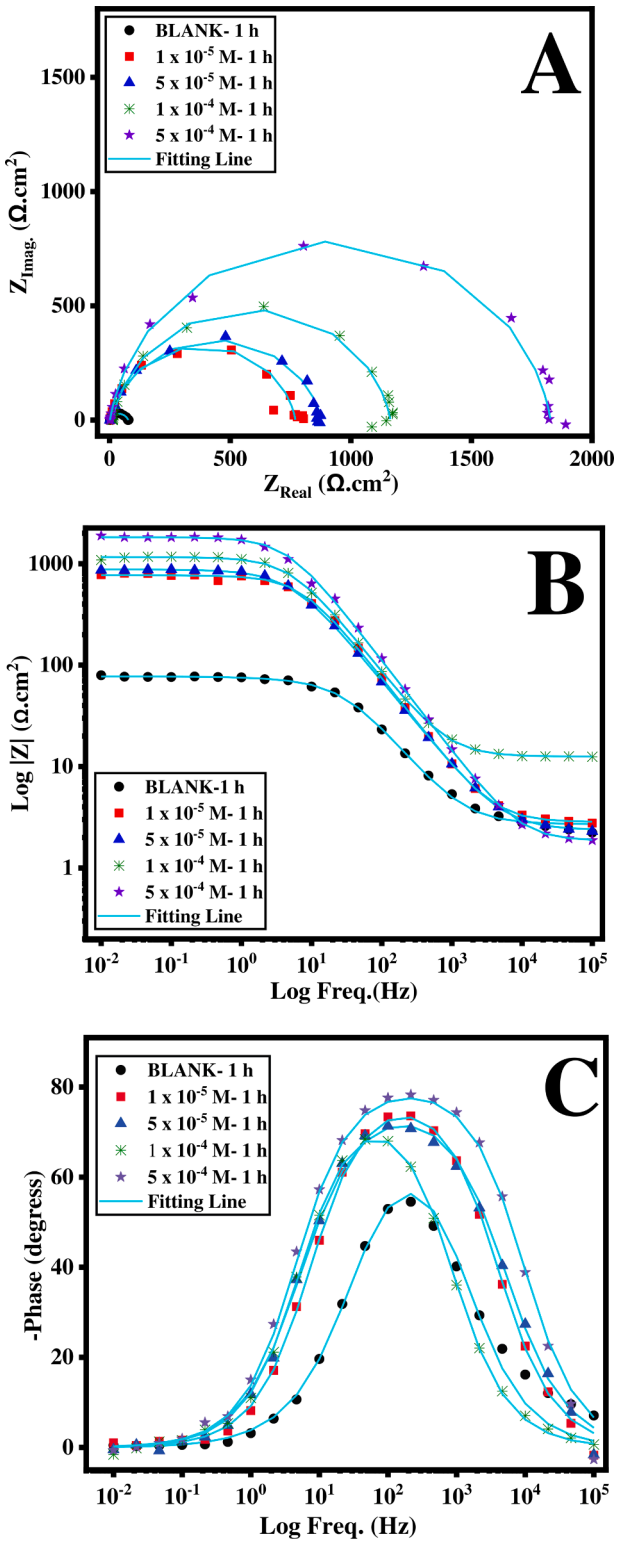

Fig. 6. Impedance spectroscopy (EIS) for uninhibited mild steel and inhibited with the presence of inhibitor MMOPH with different concentration at immersion time 1 h in 1 M HCl at 298 K, Nyquist curve (A), Bode curves (B-C).

dissolves in an acidic media with a single time constant and controlled by a charge-transfer process. As shown in Fig. 5(A), the Nyquist plots contained two depressed semicircles, especially at a high concentration of AMMP (5×10^{-4} M). A depressed semicircle indicates a more complicated model with many loops, which may be explained [19]. Furthermore, when AMMP concentration rises, the diameter of the capacitive circle grows, perhaps due to an increase in the surface coverage of adsorptive AMMP on the MS surface [62]. In Fig. 5 (B–C), the |Z| curves and Bode phase angle curves show a new evident: that for uninhibited and inhibited MS in 1 M HCl. It is widely established that corrosion resistance is determined by both the |Z| at low frequencies and the phase angle at high frequencies. In Fig. 5(B), the value of the |Z| of

the inhibited mild steel spacemen is greater than that of the uninhibited MS spacemen, indicating an exceptional efficiency of the inhibitor molecule's barriers to corrosive medium diffusion. Additionally, as shown in Fig. 5(C), the phase angle at high frequency for the inhibited MS is about 65° greater than for the mild steel without the presence of the inhibitor, indicating that the mild steel covered with the inhibitor film has stronger interfacial contact [63]. In other words, when inhibitor concentration increased, the inhibitory effectiveness increased as well. It peaked at 84.13%.

An interesting result can be seen in Fig. 6 that the Nyquist curves have a single semicircle that increases the diameter four times more than the AMMP at 5×10^{-4} M (see Fig. 6(A). Additionally, comparable behaviour was seen in Fig. 6 (B – C) in the presence of the MMOPH, but the impedance modulus and phase angle values were much higher (close to 80 ^{o}) than those obtained in the presence of the AMMP. The reason for this improvement may be due to increasing the number of nitrogen atoms and the aromatic rings in the MMOPH [23]. The highest efficiency of the inhibitor was 95.97% at a concentration 5×10^{-4} M.

In this work, all impedance spectra values of uninhibited and inhibited MS (in the existence of the AMMP and the MMOPH at an immersion time of 1,24,and 72 h) parameters were obtained by Ivium Technology (Instrument: B08024, Software: 2699 (699), throughout fitting impedance spectra curves summarized in Tables 2, and 3, respectively. Eq. (12) was used to calculate inhibitor efficiency (IE_{EIS}):

$$IE_{EIS}\ (\%) = \frac{R_{P\ (inh)} - R_{P^{\circ}}}{R_{P\ (inh)}} \times 100 \tag{12}$$

Where $R_{P^{\circ}}$ and $R_{P\ (inh)}$ denote the polarization resistance in the absence of the inhibitor and the polarization resistance in the presence of the inhibitor, respectively.

Fig.7 (a - b) shows the equivalent circuit for uninhibited and inhabited mild steel in 1 M HCl. A constant phase element (CPE) was also utilized in order to achieve an even tighter match between the experimental data sets, which was not possible with a simple equivalent circuit. The model of the equivalent circuit diagram in Fig.7(a), resistance of solution (R_S), polarization resistance (R_P) is equal to transmission of resistance charge (R_{Ct}) + diffuse layer resistance (R_d) + accumular material resistance (corrosive materials, some present molecules or ions) (R_a). At the model in Fig.7(b), R_{P1} is film resistance, R_{P2} = film resistance (R_f) + resistance referring to unprotected areas and pores (Rpor), Rpor = $R_{Ct} + R_d + R_a$, and $Rp_T = R_{P1} + R_{P2}$. Additionally, CPE_1 and CPE_2 denote the capacitance of a layer and a double layer, respectively, as calculated by Eqs. (13 and 14) [64].

$$C_l = \left(Q_1 \times R_1^{1-n} \right)^{1/n} \tag{13}$$

$$C_{dl} = \left(Q_2 \times R_2^{1-n} \right)^{1/n} \tag{14}$$

Where Q1 and Q2 denote quasi-layer capacitance and quasi-double layer capacitance, respectively, and n is the phase shift. The phase shift (n) reflects the surface shape, since a large value implies a smooth surface ($0 < n < 1$) [65]. CPE is denoted by the following expression [14].

$$Z_{CPE} = \frac{1}{Q(i\omega)^n} \tag{15}$$

Where i and ω denote, respectively, imaginary roots and angular frequency.

Tables 2-3 list the simulated values, including the Goodness of Fit (chi-square) parameter (χ^2) that describes the quality of the experimental/simulated fit. The value of χ^2 varies between 0.9 to 9.1 $\times 10^{-3}$, showing that the experimental findings are quite close to the suggested equivalent circuit [66].

According to Tables 2 and 3, the presence of the AMMP and MMOPH are increased the polarization resistance (R_p) values while decreasing the double layer capacity values (C_{dl}). These findings account for the existence of a film on the surface of the steel, confirming the two chemicals' adsorption to the metal [66].

Table 2
Electrochemical Impedance Spectroscopy (EIS) for mild steel immersion in 1 M HCl at 298 K without and with the presence of corrosion inhibitor AMMP at 1, 24, and 72 h.

Time	Concentration (M)	R_S(Ω. cm^2)	R_{p1} (Ω. cm^2)	CPE_1 (μF. cm^{-2})	n_1	R_{p2} (Ω. cm^2)	CPE_2 (μF. cm^{-2})	n_2	R_{pT} (Ω. cm^2)	Goodness of Fit ($\chi^2 \times 10^{-3}$)	% IE
1 h	BLANK	1.48 ± 0.01	37.47 ± 2	392 ± 4	0.74 ± 0.01	——	——	——-	37.47	5.6 ± 0.1	——-
	1×10^{-5}	1.05 ± 0.01	7.51 ± 1	140 ± 4	0.77 ± 0.01	62.15 ± 1	201 ± 2	0.73 ± 0.01	69.65	1.2 ± 0.1	46.21
	5×10^{-5}	1.18 ± 0.01	6.93 ± 1	124 ± 6	0.80 ± 0.01	72.84 ± 1	180 ± 2	0.77 ± 0.01	79.77	1.3 ± 0.1	53.03
	1×10^{-4}	1.06 ± 0.02	10.66 ± 2	97 ± 2	0.82 ± 0.02	94.68 ± 2	112 ± 1	0.79 ± 0.02	105.34	2.8 ± 0.2	64.43
	5×10^{-4}	0.07 ± 0.01	56.02 ± 3	52 ± 2	0.87 ± 0.02	180.07 ± 2	67 ± 1	0.81 ± 0.01	236.09	0.9 ± 0.1	84.13
24 h	BLANK	1.21 ± 0.02	15.44 ± 2	812 ± 6	0.76 ± 0.01	——	——	——	15.44	5.1 ± 0.1	——
	1×10^{-5}	0.55 ± 0.02	3.88 ± 1	212 ± 4	0.79 ± 0.01	90.76 ± 2	197 ± 2	0.81 ± 0.01	94.64	3.7 ± 0.1	83.69
	5×10^{-5}	1.49 ± 0.01	25.88 ± 1	57 ± 2	0.85 ± 0.01	125.95 ± 3	78 ± 2	0.87 ± 0.01	151.83	7.7 ± 0.2	89.83
	1×10^{-4}	0.81 ± 0.02	3.39 ± 1	42 ± 2	0.86 ± 0.01	167.62 ± 3	34 ± 1	0.89 ± 0.01	171.01	4.9 ± 0.1	90.97
	5×10^{-4}	0.99 ± 0.02	88.20 ± 2	21 ± 2	0.89 ± 0.02	284.33 ± 2	19 ± 1	0.90 ± 0.02	372.53	2.1 ± 0.1	95.86
72 h	BLANK	0.18 ± 0.02	3.43 ± 1	736 ± 6	0.71 ± 0.01	——-	——	——	3.43	9.1 ± 0.1	——-
	1×10^{-5}	0.88 ± 0.02	7.08 ± 1	288 ± 2	0.75 ± 0.01	16.38 ± 1	260 ± 2	0.77 ± 0.01	23.46	7.7 ± 0.2	85.38
	5×10^{-5}	0.81 ± 0.02	7.99 ± 1	167 ± 2	0.80 ± 0.01	23.74 ± 2	141 ± 2	0.89 ± 0.01	31.73	7.6 ± 0.2	89.19
	1×10^{-4}	0.85 ± 0.02	19.03 ± 1	56.8 ± 2	0.87 ± 0.01	40.67 ± 2	40.7 ± 1	0.90 ± 0.01	59.70	5.1 ± 0.1	94.26
	5×10^{-4}	1.21 ± 0.02	49.14 ± 3	37 ± 2	0.88 ± 0.01	107.83 ± 2	29 ± 1	0.90 ± 0.01	156.97	6.4 ± 0.2	97.82

Table 3
Electrochemical Impedance Spectroscopy (EIS) for mild steel immersion in 1 M HCl at 298 K without and with the presence of corrosion inhibitor MMOPH at 1, 24, and 72 h.

Time	Concentration (M)	R_S(Ω. cm^2)	R_{p1}(Ω. cm^2)	CPE_1 (μF. cm^{-2})	n_1	R_{p2} (Ω. cm^2)	CPE_2(μF. cm^{-2})	n_2	R_{pT}(Ω. cm^2)	Goodness of Fit ($\chi^2 \times 10^{-3}$)	% IE
	BLANK	1.48 ± 0.01	37.47 ± 2	392 ± 4	0.74 ± 0.01	—	—	——	37.47	5.6 ± 0.1	——
1 h	1×10^{-5}	1.35 ± 0.01	11.59 ± 2	43 ± 2	0.89 ± 0.01	380.32 ± 2	67 ± 2	0.89 ± 0.01	391.91	3.7 ± 0.1	90.44
	5×10^{-5}	1.33 ± 0.02	1.66 ± 1	6.31 ± 1	0.90 ± 0.01	433.88 ± 4	42 ± 2	0.90 ± 0.01	435.53	5.7 ± 0.2	91.40
	1×10^{-4}	0.55 ± 0.02	7.25 ± 1	2.2 ± 1	0.91 ± 0.02	572.78 ± 3	18 ± 1	0.91 ± 0.01	580.03	1.8 ± 0.1	93.54
	5×10^{-4}	0.36 ± 0.01	3.84 ± 1	0.7 ± 0.1	0.93 ± 0.01	926.69 ± 4	10 ± 1	0.94 ± 0.02	930.53	8.4 ± 0.2	95.97
	BLANK	1.21 ± 0.02	15.44 ± 2	812 ± 6	0.76 ± 0.01	—	——	—	15.44	5.1 ± 0.1	——
24 h	1×10^{-5}	0.60 ± 0.01	31.67 ± 2	157.6 ± 4	0.78 ± 0.01	233.23 ± 3	214 ± 4	0.82 ± 0.01	264.90	5.1 ± 0.2	94.17
	5×10^{-5}	0.55 ± 0.01	2.45 ± 1	46 ± 1	0.86 ± 0.01	275.25 ± 2	88 ± 2	0.89 ± 0.01	277.70	7.2 ± 0.2	94.44
	1×10^{-4}	0.93 ± 0.01	117.52 ± 2	27.8 ± 1	0.92 ± 0.01	192.57 ± 2	28.4 ± 2	0.91 ± 0.01	310.09	8.1 ± 0.1	95.02
	5×10^{-4}	0.70 ± 0.02	63.25 ± 2	15.2 ± 4	0.93 ± 0.01	582.82 ± 4	19.2 ± 1	0.94 ± 0.02	646.07	6.7 ± 0.2	97.61
	BLANK	0.18 ± 0.02	3.43 ± 1	736 ± 6	0.71 ± 0.01	——	—	—	3.43	9.1 ± 0.1	——
72 h	1×10^{-5}	0.35 ± 0.01	12.74 ± 1	136.7 ± 4	0.76 ± 0.02	57.28 ± 1	216 ± 3	0.77 ± 0.01	70.01	6.9 ± 0.2	95.11
	5×10^{-5}	1.01 ± 0.02	35.38 ± 1	74.54 ± 2	0.87 ± 0.02	76.15 ± 2	97 ± 2	0.78 ± 0.01	111.53	7.4 ± 0.1	96.93
	1×10^{-4}	0.64 ± 0.01	33.72 ± 2	64 ± 3	0.88 ± 0.01	95.88 ± 2	83 ± 3	0.79 ± 0.01	129.61	8.7 ± 0.2	97.35
	5×10^{-4}	1.15 ± 0.02	71.28 ± 2	39.7 ± 2	0.90 ± 0.01	146.23 ± 2	61 ± 2	0.82 ± 0.01	217.52	4.9 ± 0.1	98.43

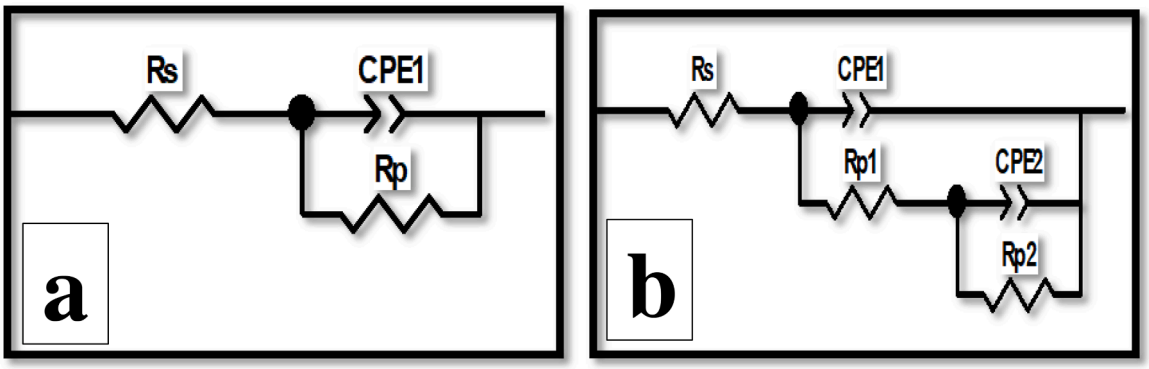

Fig. 7. Equivalent circuit for uninhibited mild steel in 1 M HCl (a), and inhibited mild steel in 1 M HCl (b). Resistance of solution (R_S), polarization resistance (R_P) is equal to transmission of resistance charge (R_{Ct}) + diffuse layer resistance (R_d) + accumular material resistance (corrosive materials, some present molecules or ions) (R_a). R_{P1} is film resistance, R_{P2} = film resistance + resistance referring to unprotected areas and pores (Rpor), Rpor = $R_{Ct} + R_d + R_a$.

The capacitance of the double layer (C_{dl}) and the thickness of the protective layer have the following relationship.

$$C_{dl} = \frac{\varepsilon \varepsilon_o S}{e} \tag{16}$$

Where, $\varepsilon, \varepsilon_o$, S and e denote the medium's dielectric constant and vacuum permittivity, the electrode's surface area, and the thickness of the protective layer, respectively [25]. The C_{dl} values (CPE_2) drop as the concentrations of the AMMP and MMOPH rise, indicating that the protective layer (e) is becoming thicker [65].

Fig.8 (A-B) shows a representative of an example of Nyquist and Bode curves with suggested models without and with the presence of inhibitor (1 M HCl + 5×10^{-4} MMOPH) by utilizing software (Ivium Technologies' CompactStat Electrochemical Interface, Instrument: B08024, Software: 2699(699)), respectively. In order to confirm the equivalent circuit model suggestion and reduce the errors, we used another software called ZView2 (version 2.90) for uninhibited and inhibited mild steel (Fig.8 (C-D).

Impedance spectroscopy supports the efficiency of polarization (MMOPH 95.97% > 84.13% AMMP). In acidic media, compounds with an increasing number of nitrogen atoms and aromatic rings are more effective than compounds with fewer nitrogen and oxygen atoms, which explains the MMOPH's superior resistance to the AMMP [67].

3.1.3. *Influence of immersion time*

EIS is a valuable method for long-term testing because it does not cause disturbance to the system and allows for tracking of its behaviour over time [68]. For 24 and 72 h at the corresponding open circuit potentials, immersion time tests were conducted with inhibited and uninhibited containing 1 M hydrochloric acid. Figs. 9 and 10 (A-C) show

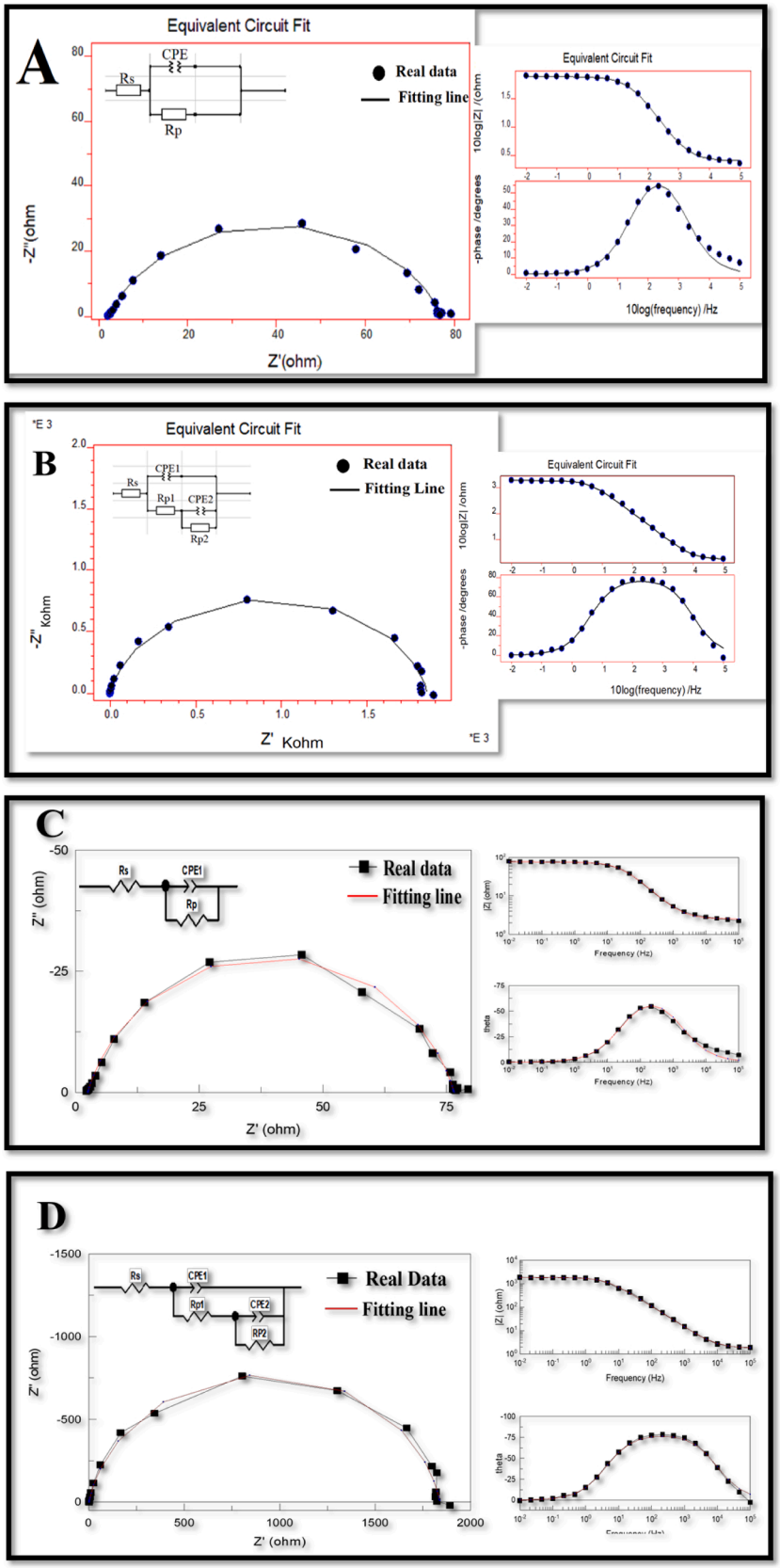

Fig. 8. Simulation example of Nyquist and Bode diagrams with suggested models for uninhibited mild steel (A and C) and with the presence of inhibitor 5×10^{-4} M MMOPH (B and D) by using Ivium software (A-B), and by using ZView 2 software (C-D).

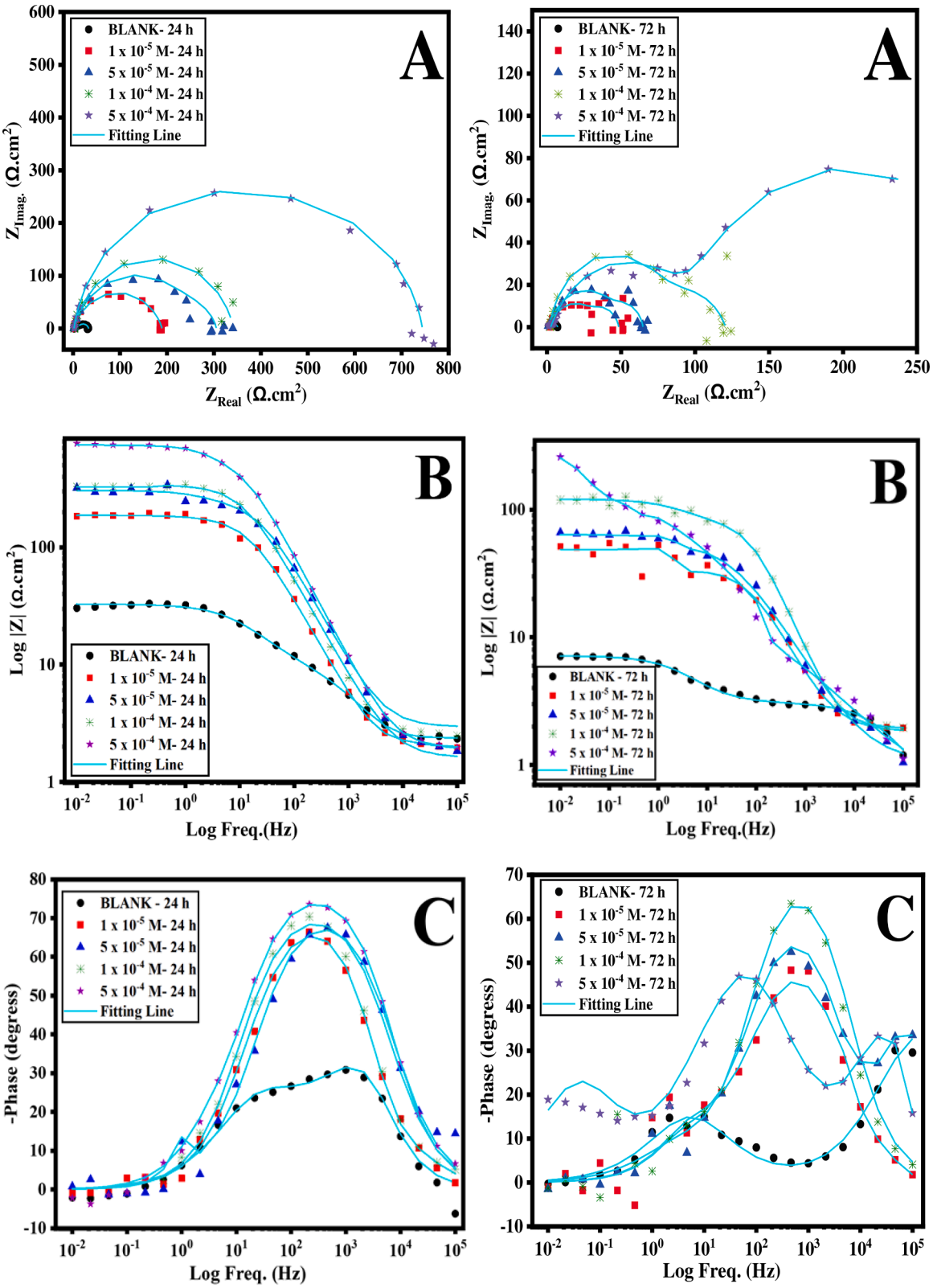

Fig. 9. Impedance spectroscopy (EIS) for uninhibited mild steel and inhibited with the presence of inhibitor AMMP with different concentration at immersion time 24 h and 72 h in 1 M HCl at 298 K, Nyquist curves (A), Bode curves (B-C).

that Nyquist curves and bode curves at immersion time 24, and 72 h for AMMP and MMOPH respectively. As shown in Fig. 9, as the time of immersion increased over 24 h, the resistance values increased significantly in the existence of inhibitor due to the increased adsorption of inhibitor molecules on the surface of MS, whereas the resistance values decreased dramatically in the absence of inhibitor. However, when the immersion period is increased to 72 h, the resistance values fall in both the blank and AMMP -containing solutions. As shown in Fig. 10, the size of impedance spectra reduces as the time interval between 24 and 72 h increases. However, overall, resistance to MS decreased slowly in the

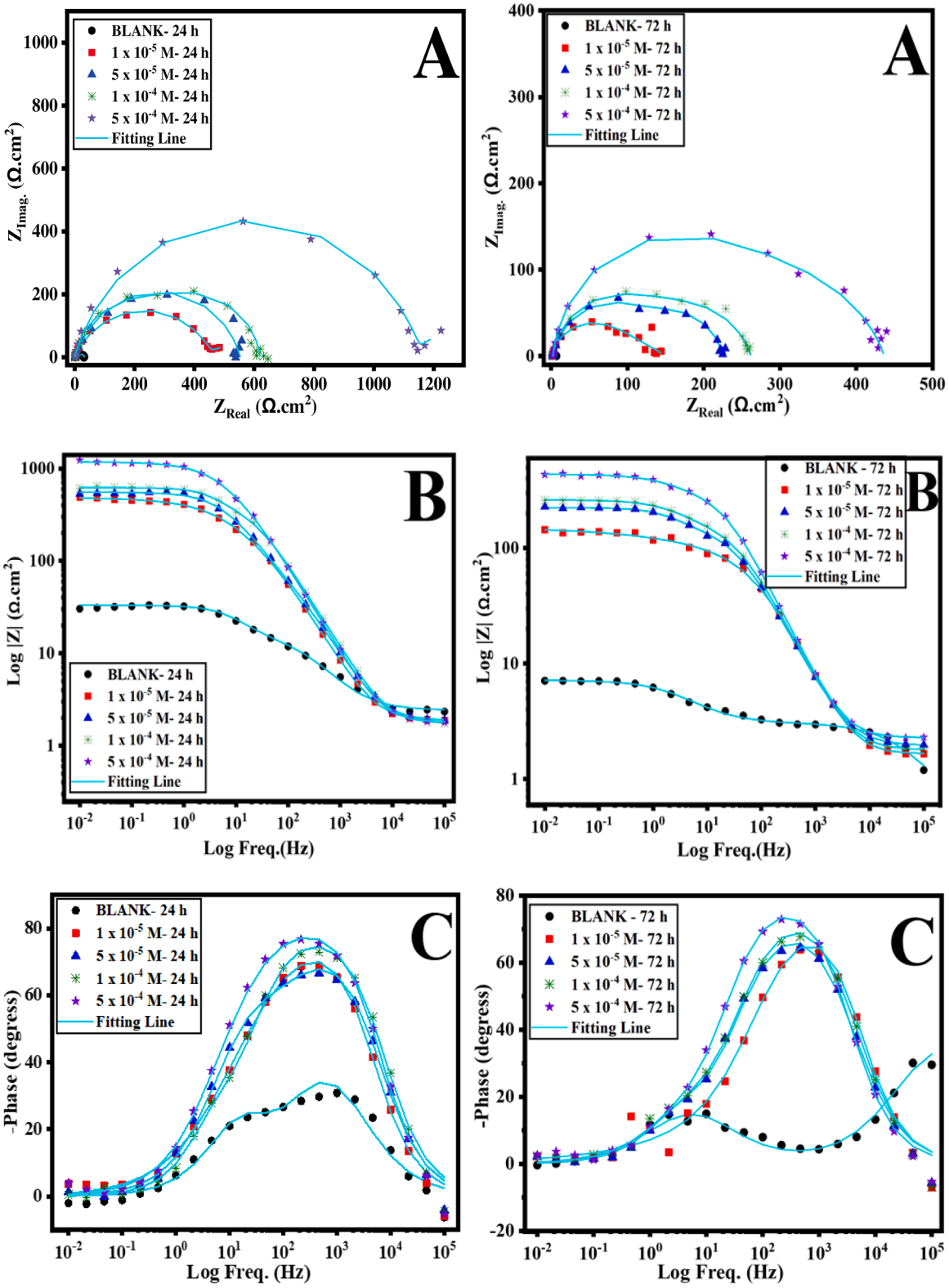

Fig. 10. Impedance spectroscopy for uninhibited mild steel and inhibited with the presence of inhibitor MMOPH with different concentration at immersion time 24, and 72 h and temperature at 298 K, Nyquist curves (A), and Bode curves (B-C).

MMOPH-containing solution as immersion time increased, while resistance without the presence of the inhibitor to MS in the 1 M HCl solution decreased sharply. The inhibition efficiency values at an immersion time of 1 h and high concentration (84.13% in the presence of the AMMP, 95.82% in the presence of the MMOPH) were lower than those between 24−72 h (95.86%–97.82% in the presence of the AMMP, and 97.61% - 98.43% in the presence of the MMOPH). This is because the adsorption process began during the first stages of immersion and continued throughout time, accumulating more particles and forming a thick layer [19]. Corrosion products may cause a layer to develop on the surface by

acting as a barrier. This film acted as a barrier to charge electron transport and contributed to the mild steel's corrosion resistance [69, 70].

3.2. Surface characterization

Fig. 11 (A-D) shows scanning electron microscopy images of mild steel before (polishing only) and after being submerged for 72 h in a 1 M hydrochloric acid solution without and with the presence 5×10^{-4} of inhibitors AMMP and MMOPH, respectively. Fig. 11(A) illustrates a

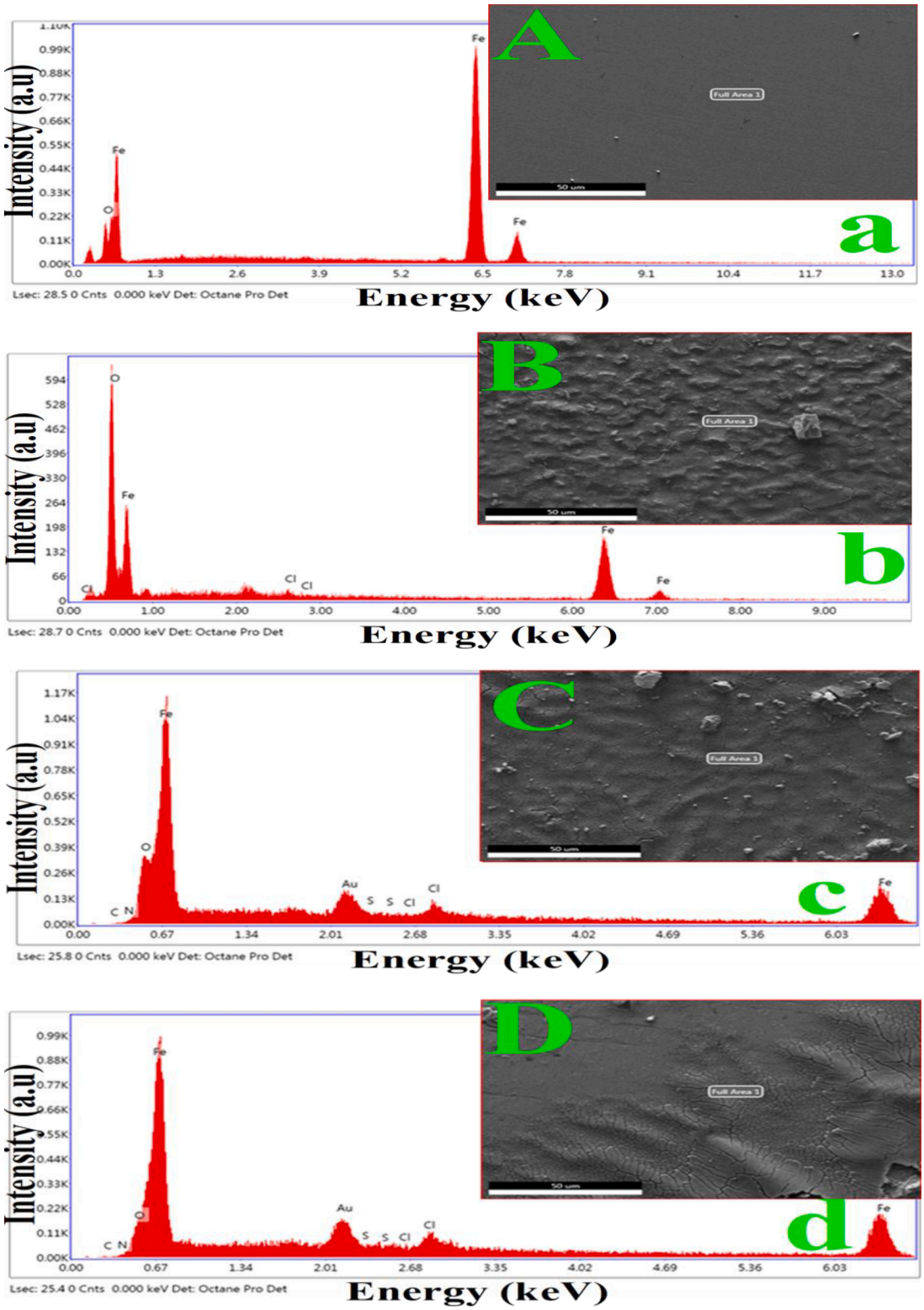

Fig. 11. SEM (A-D) and EDX (a-d) images of mild steel surface before (A-a; polishing) and after immersion 72 h in 1 M HCl solution at 298 K in the absence and existence of 5×10^{-4} M of inhibitors: (B-b; blank), (C-c; AMMP), (D-d; MMOP).

corrosion-free surface with a smooth surface and a few parallel scratch lines from the polishing process. Without an inhibitor, the surface corrosivity is extremely high, as illustrated in Fig. 11(B), attributable to the mild steel's comparatively high susceptibility to the fast corrosion process in an aggressive HCl solution. However, when treated with 5×10^{-4} M of AMMP Fig. 11(C) and MMOPH Fig. 11(D) in 1 M HCl, a mild steel sample provides much superior outcomes in terms of the morphology of the hindered surface, which is smoother when compared to the uninhibited surface. In contrast, the mild steel surface exhibits much less corrosion and is significantly more homogenous in the presence of MMOPH. The electrolyte is stopped from entering the mild steel by creating a protective film on the surface.

Energy dispersive X-ray spectroscopy (EDX) tests were also performed to ascertain the presence of various elements on the surface of the examined samples. Fig. 11 (a-d) illustrates the EDX spectra of MS before (polishing only) and after immersion for 72 h in a 1 M HCl

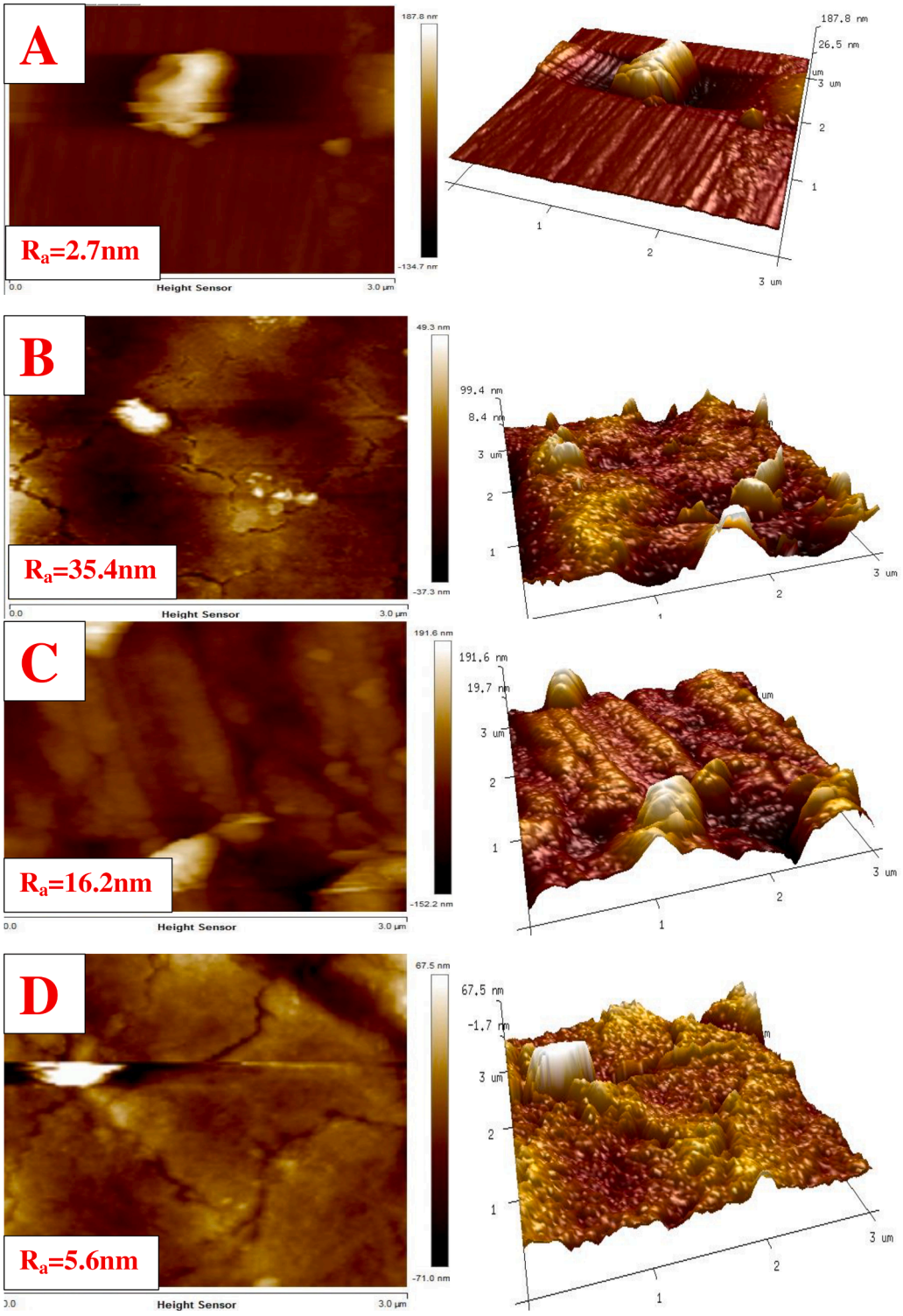

Fig. 12. AFM images of mild steel surface before (A- polishing) and after immersion 72 h in 1 M HCl solution at 298 K in the absence and existence of 5×10^{-4} M of inhibitors: (B-blank), (C-AMMP), (D-MMOPH).

solution without and with the presence of 5×10^{-4} of inhibitors AMMP and MMOPH, respectively. As shown in Fig. 11(a), the EDX spectrum revealed a free corrosion surface with a high peak for iron and a low peak for oxygen. By interpreting the spectrum (b), it is clear that iron oxide is created through corrosion-induced processes; this is shown by the existence of a high oxygen peak in the mild steel EDX spectra of the blank. In addition, after 72 h of immersion, it is important to note the existence of the Cl peak that indicates the presence of this element on the surface attributed to the reason that it comes from the HCl solution in the sample. When comparing the spectrums (c) and (d) to the blank, we observe a reduction in the oxygen peak. In addition, the Au peak observed in the EDX spectra (Fig.11 (c and d) is due to the coating applied to the surface in order to obtain high resolution images from SEM measurements and to perform EDX analysis under high voltage (see Section 2.4). The results also show a significant reduction in MMOPH. This demonstrates the compounds' inhibitory properties by their capacity to create a preventative layer on the surface of the MS, preventing electrolyte access and therefore minimizing the corrosion phenomena [68,69].

Fig. 12 (A-D) shows AFM images of 2D and 3D of MS surface before (polishing only) and after immersion for 72 h in 1 M HCl solution in the absence and existence of 5×10^{-4} M of inhibitors AMMP, MMOPH, respectively. As can be noticed in Fig. 12(A), the surface prior to immersion is very smooth and uncorroded, with an average surface roughness (R_a) of 2.7 nm. However, it can be noted that the surface submerged in 1 M HCl (Fig. 12(B) shows obvious signs of corrosion, with very high roughness and a damaged surface owing to the presence of acidic solution, and the Ra value is 35.4 nm, indicating that the surface has been damaged by corrosion due to attack the surface by aggressive ions like Cl^- and H^+ ions. Comparing Fig. 12(C) to Fig. 12(B), it can be observed that the surface is less roughness and has a Ra value of 16.2 nm, which is due to the existence of the inhibitor AMMP adsorbed on the surface, which inhibits aggressive ions from attacking the surface Fig. 12 (D) shows the best result when compared to Fig. 12(B)-(C), and the R_a value is 5.6 nm. This is owing to the presence of the inhibitor MMOPH, which provided the best result when compared to Fig. 12(B)-(C). Therefore, the lower R_a values for the inhibited sample indicate that the surface is less roughness due to the formation of a thin layer on the mild steel surface as a result of adsorption of the inhibitor molecules onto the MS surface [23].

On the basis of SEM, EDX, and AFM observations, it can be concluded that the AMMP and MMOPH have a strong propensity to adsorb on the MS surface, which is matched with electrochemical studies.

3.3. Adsorption isotherm

The organic inhibitors' inhibitive effect in 1 M HCl solution is mostly due to their adsorption on the metal surface of the metal. The inhibition efficiency (IE_{LPR} (%)) was utilized to calculate the surface coverage (θ), where θ is equal to IE_{LPR} (%)/100. In the literature, there are a number of adsorption isotherms recognized by scientists, and the Langmuir isotherm has been demonstrated to be more suitable for this scenario [71].

$$\frac{C_{inh}}{\theta} = \frac{1}{K_{ads}} + C_{inh} \tag{17}$$

Where C_{inh}, θ and K_{ads} denote the inhibitor concentration, respectively, the inhibitor's surface coverage and the equilibrium constant for the adsorption – desorption process [72].

The graph of C_{inh}/θ versus C_{inh} is given in Fig. 13; it conforms to the Langmuir isotherm's adsorption model. Table 4 contains the characteristics derived from Fig. 13. The ΔG_{ads} can be determined by utilizing the equation below:

$$\Delta G_{ads} = -RT\ln(55.5K_{ads}) \tag{18}$$

Where R and T denote the gas constant and absolute temperature,

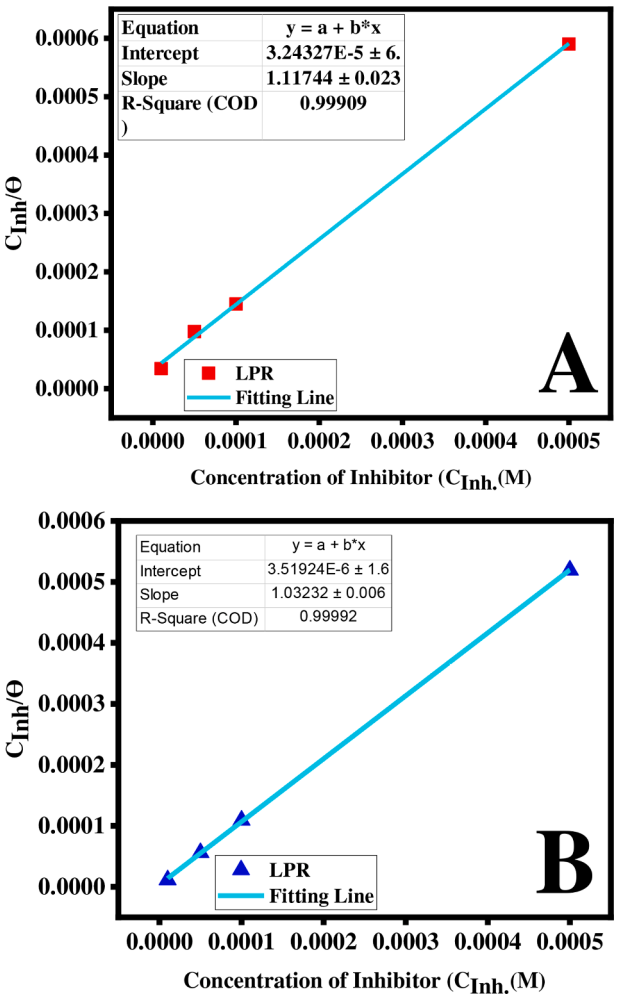

Fig. 13. Langmuir adsorption isotherm for mild steel with presence, AMMP (A), MMOPH (B).

Table 4
Langmuir adsorption parameters of AMMP and MMOPH on mild steel surface in 1 M HCl solution at 298 K.

Corrosion Inhibitor	K_{ads} (M^{-1})	Slope	ΔG kJ/mol
AMMP	30,833.08	1.11744 ± 0.02389	- 35.6
MMOPH	284,155.49	1.03232 ± 0.00648	- 41.1

respectively, and 55.5 denotes the solution concentration of H_2O in mol/L [73].

If ΔG^o_{ads} is below or equal to 20 kJ.mol^{-1}, this is a case of physisorption involving electrostatic interactions between the charged metal and the charged inhibitor. Chemisorption happens when the absolute value of ΔG^o_{ads} exceeds or equals 40 kJ.mol^{-1}; this is a charge transfer between the metal surface and the inhibitor molecules [74–76]. According to the results, the value of ΔG^o_{ads} for AMMP is - 35.6 kJ.mol^{-1}, which can classify the adsorption as physisorption and chemisorption. However, the value for MMOPH is - 41.1 kJ.mol^{-1}indicated that the adsorption may classify as chemisorption.

On the other hand, Table. 5 illustrates the comparison of the inhibitory efficacy of previously reported compounds to that of the chemicals examined in this research (AMMP and MMOPH). The inhibitory efficiency values in this table were determined by measuring EIS following immersion in various solutions. By comparing these results, we are able to demonstrate that our compounds are the most efficient HCl inhibitors. Moreover, we can see from Table 5 that the heteroatoms and phenyl

Table 5
Comparison of the inhibitory efficacy of previously reported compounds to that of the chemicals examined in this research (AMMP and MMOPH).

Corrosion inhibitor	Metal	No. N atom	No. S atom	Efficiency %	Reference
4,6-dimethylpyrimidine-2-amine	Carbon steel	3	–	71.2	[82]
N-benzylidene-4,6-dimethylpyrimidin-2-amine	Carbon steel	3	–	92.7	[82]
7-methoxypyrido [2,3-d]pyrimidine-4-amine	Mild steel	4	–	97.6	[44]
1,2,4-triazolo[1,5-*a*] pyrimidine derivatives	Mild steel	5	–	93.0	[83]
AMMP	Mild steel	3	1	84.1	This work
MMOPH	Mild steel	4	1	95.9	This work

rings played a good role in the improvement of inhibitor efficiency [23].

3.4. Density functional theory calculations (DFT)

Typically, inhibitor active sites may be deduced using frontier molecular orbital theory. As a result, DFT simulations were used to examine the connection between molecular structure and corrosion inhibition efficacy in this work. The HOMO and LUMO values are the two most critical parameters in the theoretical section. The HOMO (highest occupied molecular orbital) value is proportional to the ability of the molecule to donate an electron to the metal surface's vacant d-orbital, i.e., the more significant the molecule, the higher its ability to donate. While the LUMO (lowest unoccupied molecular orbital) value is inversely proportional to the electron acceptance ability, the lower its value, the more readily its electron adopts the inclination from the metal orbital. The optimized structure, HOMO, LUMO, and molecule electrostatic potential (ESP) for AMMP and MMOPH are shown in Fig. 14. In both compounds, the HOMO energy is shown to be located on the heteroatoms (S = C—N group, NH_2 group) as illustrated in Fig. 14. However, the HOMO energy for MMOPH (−6.204 eV) is greater than the HOMO energy for AMMP (−6.567 eV), indicating that MMOPH's inhibitor is more effective than AMMP's. Moreover, as shown in Fig.14, the E_{LUMO} energy is found on the phenyl ring and the majority of heteroatoms in both compounds, although the LUMO energy for MMOPH (−2.255 eV) is lower than the E_{LUMO} energy for AMMP (−2.200 eV). Another aspect is that, according to the literature, MMOPH is more efficient than AMMP. As a result, they are the preferred locations for interacting with the metal surface. This is further supported by the ESP illustration. The red area in Fig. 14 (ESP) represents electrophilicity, whereas the blue area represents nucleophilicity. S and O atoms, which are more likely to make covalent connections with Fe-d orbitals, dominate the red areas [77,78].

In general, a decrease in the ΔE (Table.6) leads to easier molecular polarization, greater surface adsorption, and better inhibitor performance. In other words, the energy gap for MMOPH (3.945 eV) is smaller than the energy gap for AMMP (4.367 eV), which is highly supported by the experimental evidence [41]. Furthermore, Table.6 shows the fraction of transferred electrons (ΔN) which is an essential parameter for evaluating the inhibition performance. According to the literature, increasing the inhibition effectiveness to a value of $\Delta N < 3.6$ enhances the ability to sacrifice electrons to the metal surface [79].

In an aqueous environment, the inhibitor molecule is protonated, and the protonated molecules are adsorbed on the mild steel surface. As a result, a comparison of the electrical properties of protonated and neutral species is required to determine which adsorbents are often produced on the metal surface. Fig.15 shows the protonated form of the molecule for quantum chemical results of AMMP and MMOPH molecules determined by using Gaussian 09 software at B3LYP-6–311 in water phase at 298 K. It can be seen from Fig. 15 that the sulfur atom in both compounds is a more preferential site for protonation than that of the other atoms. As shown in Table 6, the energy gap values (ΔE) for both compounds are smaller for their protonated forms ($AMMPH^+$ and $MMOPHH^+$) when compared to their neutral forms (AMMP and MMOPH). This means that the protonated state is more reactive than the neutral state. As a result, protonated versions of the compounds are more prone to adsorb on mild steel surfaces [16]. The above statement provides further confirmation of the experimental adsorption. In other words, quantum chemical calculations are very compatible with experimental data, and both compounds exhibit inhibitory activity of the order of MMOPH > AMMP.

3.5. Monte Carlo simulation (MC)

The adsorption behaviour of the inhibitors on the Fe (110) surface was investigated using Monte Carlo simulations, while also taking into account the conditions in which the tests were performed (the existence of the tested compounds in a HCl solution). On the 150 H_2O + 3 H_3O^+ + 3 Cl^- / Fe (110) molecule system, Fig. 16 illustrates the much steadier low–energy adsorption features of inhibitors. Table 7 lists the adsorption energies of the inhibitors tested on the Fe (110) / inhibitor system. As shown in Fig. 16, the studied inhibitor molecules were preferentially vertical and formed an umbrella-like cover on the Fe surface, maximizing interaction and increasing the surface protection. The strong contact between the phenyl rings of inhibitor substances and the metal surface is responsible for this adsorption paradigm. Furthermore, these results show that the N, S, and O atoms have strong interaction with one other as well as with many π-electrons, and the metal surface, which may provide the empty orbital electrons of iron coordinate bonds to form. As a consequence, MCS verified the inhibitors' adsorption and the formation of a steady barrier layer on the MS surface. The values of the investigated inhibitors' adsorption energies on the simulated system are in the following order: MMOPH > AMMP. The electrochemical and surface characterization findings support this order as well [33,57,80].

3.6. Mechanism of corrosion inhibition

After studying the anticorrosive properties of the two substances in an acidic media utilizing experimental techniques and verifying them theoretically on the surface of mild steel in the previous section, the goal of this section is to simplify the adsorption mechanism of the more efficient molecule, while considering the various components that take place in the solution. Recent research has shown that the compounds under investigation are high-performance corrosion inhibitors with outstanding electronic characteristics. The estimate of the adsorption process may be described in the manner shown in Fig. 17. Cathodic and anodic reaction processes may be seen as bellowing in the absence and presence of AMMP and MMOP molecules [17,76,81].

Anodic reactions:

$$Fe + nH_2O \rightarrow Fe(H_2O)_n \quad (19)$$

$$Fe(H_2O)_n + 2Cl^- \rightarrow Fe[H_2O_n 2Cl^-] \quad (20)$$

$$Fe[H_2O_n 2Cl^-] + [MMOPH]^+ \rightarrow Fe[H_2O_n 2Cl^-][MMOPH]^+ \quad (21)$$

$$Fe[H_2O_n 2Cl^-][MMOPH]^+ + e^- \rightarrow \left[Fe(H_2O)_n 2Cl^- MMOPH\right]^- \quad (22)$$

Cathodic reactions:

$$H^+ + e^- \rightarrow \frac{1}{2}H_2 \quad (23)$$

$$Fe + [MMOPH]^+ \rightarrow (Fe[MMOPH]^+ \quad (24)$$

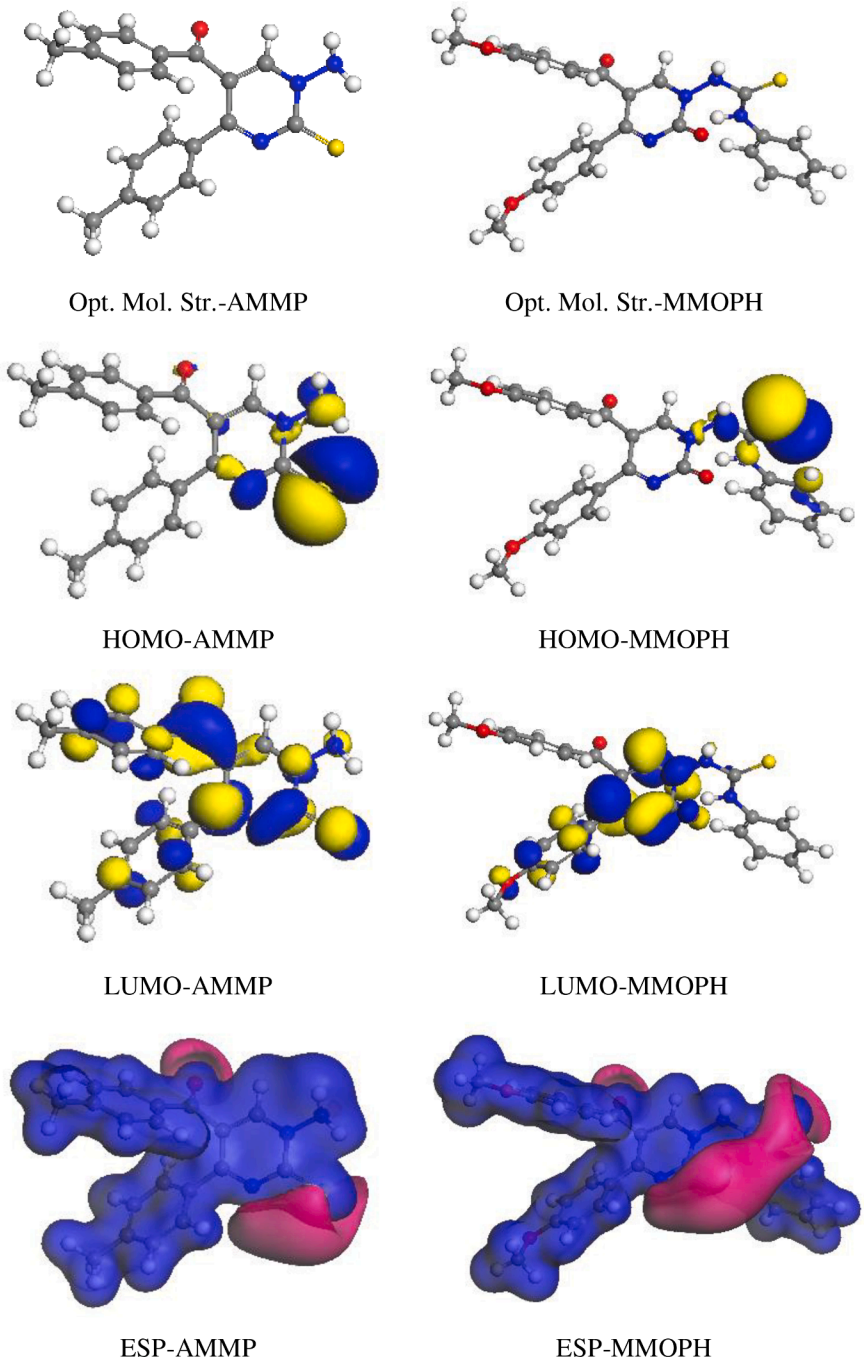

Fig. 14. Optimized structure, HOMO, LUMO, and molecular electrostatic potential (ESP) for quantum chemical results of AMMP and MMOPH molecules using the DMol3 module in Material Studio 2017 (Method: GGA/BLYP; Basis set: DNP 3.5; Solvation model: COSMO).

Table 6
Density function theory parameters for AMMP and MMOPH by using Gaussian 09 software at B3LYP-6–311 in water phase at 298 K.

Molecule	E_{HOMO} (eV)	E_{LUMO} (eV)	ΔE (eV)	η (eV)	χ (eV)	ΔN (eV)
AMMP	−6.567	−2.200	4.367	2.184	4.384	0.5989
$AMMPH^+$	−9.616	−6.124	3.492	1.746	7.870	0.2491
MMOPH	−6.204	−2.255	3.949	1.975	4.229	0.7015
$MMOPHH^+$	−8.195	−5.241	2.955	1.477	6.718	0.0954

$$Fe[MMOPH]^+ + e^- \rightarrow (Fe[MMOPH]) \quad (25)$$

The breakdown of mild steel without the presence of AMMP and MMOPH molecules is described in Eqs. (19) and 20. While Eqs. (21) and 22 relate to the existence of inhibitor molecules that cause anodic dissolution to be slowed down as a result of their adsorption on the surface. In the absence of AMMP and MMOPH molecules, hydrogen evolution was the main cathodic process, as seen above (Eq. (23)). According to Eqs. (24) and 25, the presence of a positively charged [MMOPH] + group in the investigated compounds adsorbs on the cathodic sites of the MS, resulting in a slower rate of H_2 evolution. Increased surface iron oxidation produces an aggressive acid solution and/or negatively charged chemicals ([AMMP] and [MMOPH]

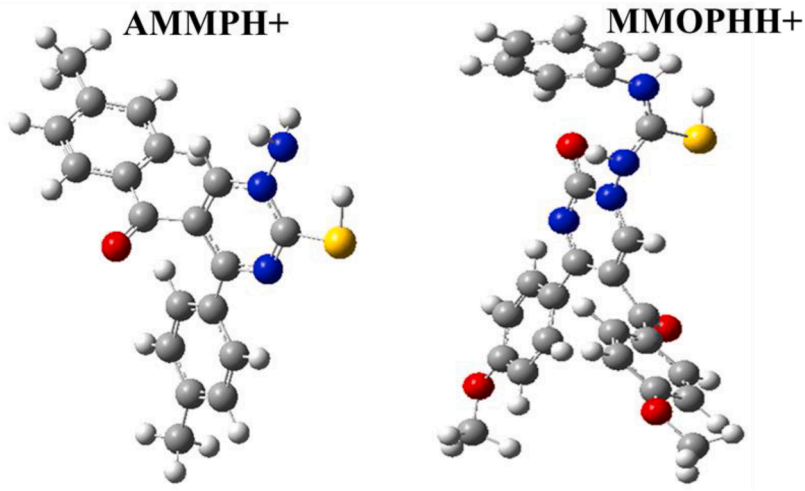

Fig.15. The protonated form of the molecule for quantum chemical results of AMMP and MMOPH molecules determined by using Gaussian 09 software at B3LYP-6–311 in water phase at 298 K.

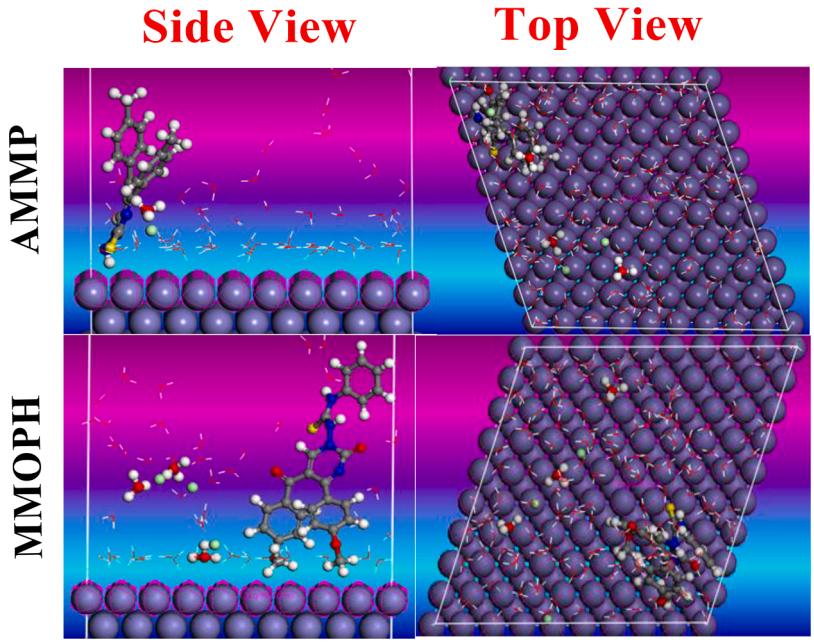

Fig. 16. Top and side views of the equilibrium configuration for AMMP and MMOPH adsorbed on Fe (1 1 0) in aqueous system simulated by Material Studio (2017)'s adsorption locator module at 298 K.

Table 7
Adsorption energies of AMMP and MMOPH inhibitors adsorbed on Fe (110) surface measured by Material Studio (2017)'s adsorption locator module at 298 K.

Complex	Adsorption energy E_{ads} (kcal. mol^{-1})	Binding energy$E_{binding}$ (kcal. mol^{-1})
AMMP@ Fe (110)	−48.271	48.271
MMOPH@ Fe (110)	−69.027	69.027

molecules) that bind negative charges to ions. By electrostatic attraction, the negatively charged metallic surface attracts positive cationic movement, resulting in the physiosorbed [AMMP] and [MMOPH] molecules. Adsorbed inhibitor molecules ([AMMP] and [MMOPH]) may, however, react with π-electron that are not attached and chemisorbed, resulting in a reaction. Thus, [AMMP] and [MMOPH] molecules are adsorbed at metal-electrolyte contacts through physisorption and subsequently chemisorption. It is thought that adsorbing inhibitor molecules transfer electrons from their empty anti-bonding molecular orbitals to the surface orbitals of iron atoms and recognize electrons, thus increasing interactions with the metal surface [34] (see Fig. 17).

Conclusion

The following conclusion can be drawn according to the collected data:

1- Both compounds, AMMP and MMOPH appeared excellent corrosion inhibitors. However, MMOPH (IE = 95.97% at immersion time 1 h) is better than AMMP (IE= 84.13% at immersion time 1 h).

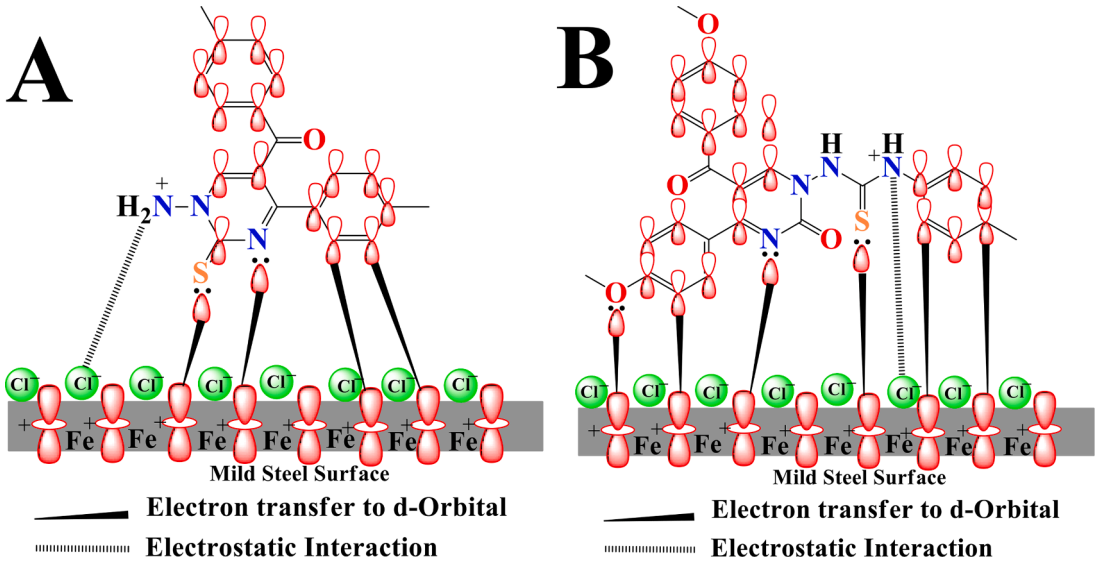

Fig. 17. schematic the mechanism of corrosion inhibitor, in case presence of AMMP (A), in case presence of MMOPH (B).

2- The current density was reduced with the presence of inhibitors from 517.93 to 56.18 and 9.96 μA.cm^{-2} at 5 × 10^{-4} M for AMMP and MMOPH, respectively according to PDP results.
3- A Langmuir adsorption model is the best match for the adsorption of AMMP and MMOPH molecules on the MS surface.
4- Tafel curves reveal that AMMP and MMOPH function without altering the mechanism of hydrogen evolution as a mixed type inhibitor.
5- The equivalent circuits for EIS plots without and with the existence of inhibitors have been approved by another software called ZView 2. With the existence of AMMP and MMOPH in acid solution, the polarization resistance increases thus decreasing double layer capacitance as a result of the rise in the thickness of the electrical double layer.
6- SEM and EDX results confirm the present of molecules of inhibitor on the surface of mild steel, While the average surface roughness value (Ra) was reduced from 35.4 nm to 16.2 and 5.6 nm with the presence of AMMP and MMOPH, respectively, confirmed by AFM images.
7- Density function theory calculation (DFT) and MC simulation verified the inhibitors' adsorption and the formation of a stable barrier layer on the Fe (110) surface and the absolute values of the investigated inhibitors' E_{ads} on the simulated system are in the following order: MMOPH > AMMP. In addition, the sulfur atom in both compounds is a more preferential site for protonation than that of the other atoms.

Acknowledgement

The authors want to express their gratitude to the Scientific Research Coordination Unit of Kastamonu University. This study was supported financially by the KÜ-BAP03/2020-5 project. ***Mothana Ghazi Kadhim AlFalah*** also thanks Materials of Engineering department, college of Engineering, University of Al- Qadisiyah, Iraq, for giving opportunity to complete his study throughout PhD programme.

References

[1] M. Goyal, H. Vashisht, S. Hamed Alrefaee, R. Jain, S. Kumar, S. Kaya, L. Guo, C. Verma, Decyltriphenylphosphonium bromide containing hydrophobic alkyl-chain as a potential corrosion inhibitor for mild steel in sulfuric acid: theoretical and experimental studies, J. Mol. Liq. (2021) 336, https://doi.org/10.1016/j.molliq.2021.116166.
[2] M. Mahdavian, S. Ashhari, Electrochimica Acta Corrosion inhibition performance of 2-mercaptobenzimidazole and 2-mercaptobenzoxazole compounds for protection of mild steel in hydrochloric acid solution, 55 (2010) 1720–1724. https://doi.org/10.1016/j.electacta.2009.10.055.
[3] M. Murmu, S.K. Saha, P. Bhaumick, N.C. Murmu, H. Hirani, P. Banerjee, Corrosion inhibition property of azomethine functionalized triazole derivatives in 1 mol L−1 HCl medium for mild steel: experimental and theoretical exploration, J. Mol. Liq. (2020), 113508, https://doi.org/10.1016/j.molliq.2020.113508.
[4] C. Verma, I.B. Obot, I. Bahadur, E.S.M. Sherif, E.E. Ebenso, Choline based ionic liquids as sustainable corrosion inhibitors on mild steel surface in acidic medium: gravimetric, electrochemical, surface morphology, DFT and Monte Carlo simulation studies, Appl. Surf. Sci. 457 (2018) 134–149, https://doi.org/10.1016/j.apsusc.2018.06.035.
[5] M.G.K. AlFalah, M.T. Ali, A critical review on corrosion and its prevention in the oilfield equipment, J. Pet. Res. Stud. 7 (2017) 162–189, https://doi.org/10.52716/jprs.v7i2.195.
[6] A. Chaouiki, M. Chafiq, H. Lgaz, M.R. Al-Hadeethi, I.H. Ali, S. Masroor, I.M. Chung, Green corrosion inhibition of mild steel by hydrazone derivatives in 1.0M HCl, Coatings 10 (2020) 0–17, https://doi.org/10.3390/coatings10070640.
[7] H. Ferkous, S. Djellali, R. Sahraoui, Y. Benguerba, H. Behloul, A. Çukurovali, Corrosion inhibition of mild steel by 2-(2-methoxybenzylidene) hydrazine-1-carbothioamide in hydrochloric acid solution: experimental measurements and quantum chemical calculations, J. Mol. Liq. 307 (2020), 112957, https://doi.org/10.1016/j.molliq.2020.112957.
[8] L. Tabti, R.M. Khelladi, N. Chafai, A. Lecointre, A.M. Nonat, L.J. Charbonnière, E. Bentouhami, Corrosion protection of mild steel by a new phosphonated pyridines inhibitor system in HCl solution, Adv. Eng. Forum. 36 (2020) 59–75, https://doi.org/10.4028/www.scientific.net/aef.36.59.
[9] S. Bashir, V. Sharma, H. Lgaz, I.M. Chung, A. Singh, A. Kumar, The inhibition action of analgin on the corrosion of mild steel in acidic medium: a combined theoretical and experimental approach, J. Mol. Liq. 263 (2018) 454–462, https://doi.org/10.1016/j.molliq.2018.04.143.
[10] D. Özkır, K. Kayakırılmaz, The inhibitor effect of (E)-5-[(4-(*benzyl*(*methyl*)*amino*)*phenyl*)*dia-zenyl*]-1,4-dimethyl-1h-1,2,4-triazol-4-ium zinc(ii) chloride, an industrial cationic azo dye, onto reducing acidic corrosion rate of mild steel, J. Electrochem. Sci. Technol. 11 (2020) 257–272, https://doi.org/10.33961/jecst.2019.00703.
[11] A.K. Singh, B. Chugh, S.K. Saha, P. Banerjee, E.E. Ebenso, S. Thakur, B. Pani, Evaluation of anti-corrosion performance of an expired semi synthetic antibiotic cefdinir for mild steel in 1 M HCl medium: an experimental and theoretical study, Results Phys 14 (2019), 102383, https://doi.org/10.1016/j.rinp.2019.102383.
[12] C.B.P. Kumar, K.N. Mohana, M.S. Raghu, M.B. Jagadeesha, M.K. Prashanth, N. K. Lokanath, Mahesha, Fluorine substituted thiomethyl pyrimidine derivatives as efficient inhibitors for mild steel corrosion in hydrochloric acid solution: thermodynamic, electrochemical and DFT studies, J. Mol. Liq. 311 (2020), 113311, https://doi.org/10.1016/j.molliq.2020.113311.
[13] M. Chafiq, A. Chaouiki, M.R. Albayati, H. Lgaz, R. Salghi, S.K. AbdelRaheem, I. H. Ali, S.K. Mohamed, I.M. Chung, Unveiled understanding on corrosion inhibition mechanisms of hydrazone derivatives based on naproxen for mild steel in HCl: a joint experimental/theoretical study, J. Mol. Liq. (2020) 320, https://doi.org/10.1016/j.molliq.2020.114442.
[14] M. Rbaa, M. Ouakki, M. Galai, A. Berisha, B. Lakhrissi, C. Jama, I. Warad, A. Zarrouk, Simple preparation and characterization of novel 8-Hydroxyquinoline derivatives as effective acid corrosion inhibitor for mild steel: experimental and theoretical studies, Colloids Surfaces A Physicochem. Eng. Asp. 602 (2020), 125094, https://doi.org/10.1016/j.colsurfa.2020.125094.
[15] D. quan Zhang, Z. xun An, Q. yi Pan, L. xin Gao, G. ding Zhou, Comparative study of bis-piperidiniummethyl-urea and mono-piperidiniummethyl-urea as volatile

corrosion inhibitors for mild steel, Corros. Sci. 48 (2006) 1437–1448, https://doi.org/10.1016/j.corsci.2005.06.007.
[16] S. Rameshkumar, I. Danaee, M. RashvandAvei, M. Vijayan, Quantum chemical and experimental investigations on equipotent effects of (+)R and (-)S enantiomers of racemic amisulpride as eco-friendly corrosion inhibitors for mild steel in acidic solution, J. Mol. Liq. 212 (2015) 168–186, https://doi.org/10.1016/j.molliq.2015.09.001.
[17] D. Daoud, T. Douadi, H. Hamani, S. Chafaa, M. Al-Noaimi, Corrosion inhibition of mild steel by two new S-heterocyclic compounds in 1M HCl: experimental and computational study, Corros. Sci. 94 (2015) 21–37, https://doi.org/10.1016/j.corsci.2015.01.025.
[18] M.E. Belghiti, Y. Karzazi, S. Tighadouini, A. Dafali, C. Jama, I. Warad, B. Hammouti, S. Radi, New hydrazine derivatives as corrosion for mild steel in phosphoric acid medium. Part B: theoretical investigation, J. Mater. Environ. Sci. 7 (2016) 956–967.
[19] H. Keleş, M. Keleş, K. Sayın, Experimental and theoretical investigation of inhibition behaviour of 2-((4-(dimethylamino)benzylidene)amino)benzenethiol for carbon steel in HCl solution, Corros. Sci. (2021) 184, https://doi.org/10.1016/j.corsci.2021.109376.
[20] N. Arrousse, R. Salim, Y. Kaddouri, A. zarrouk, D. Zahri, F. El Hajjaji, R. Touzani, M. Taleb, S. Jodeh, The inhibition behaviour of two pyrimidine-pyrazole derivatives against corrosion in hydrochloric solution: experimental, surface analysis and in silico approach studies, Arab. J. Chem. 13 (2020) 5949–5965, https://doi.org/10.1016/j.arabjc.2020.04.030.
[21] M. Abd El-Raouf, E.A. Khamis, M.T.H. Abou Kana, N.A. Negm, Electrochemical and quantum chemical evaluation of new bis(coumarins) derivatives as corrosion inhibitors for carbon steel corrosion in 0.5M H_2SO_4, J. Mol. Liq. 255 (2018) 341–353, https://doi.org/10.1016/j.molliq.2018.01.148.
[22] M. Ghazi, Mothana G.K. Alfalah, M. Abdulrazzaq, M. Saracoglu, F. Kandemirli, 4-naphthyl-3-thiosemicarbazide as corrosion inhibitor for copper in sea water (3.5% soduim chloride), Eurasian J. Sci. Eng. Technol. 1 (2020) 27–34.
[23] N. Mohanapriya, M. Kumaravel, B. Lalithamani, Theoretical and experimental studies on the adsorption of n-[(E)-pyridin-2-ylmethylidene] aniline, a schiff base, on mild steel surface in acid media, J. Electrochem. Sci. Technol. 11 (2020) 117–131, https://doi.org/10.33961/jecst.2019.00430.
[24] P. Leena, N.H. Zeinul Hukuman, A.R. Biju, M. Jisha, Studies on methanolic extract of lepidagathis keralensis as green corrosion inhibitor for mild steel in 1M HCL, J. Electrochem. Sci. Technol. 10 (2019) 231–243, https://doi.org/10.5229/JECST.2019.10.2.231.
[25] Z. Rouifi, M. Rbaa, A.S. Abousalem, F. Benhiba, T. Laabaissi, H. Oudda, B. Lakhrissi, A. Guenbour, I. Warad, A. Zarrouk, Synthesis, characterization and corrosion inhibition potential of newly benzimidazole derivatives: combining theoretical and experimental study, Surf. Interfaces 18 (2020), https://doi.org/10.1016/j.surfin.2020.100442.
[26] V. Saraswat, M. Yadav, I.B. Obot, Investigations on eco-friendly corrosion inhibitors for mild steel in acid environment: electrochemical, DFT and Monte Carlo Simulation approach, Colloids Surf. A Physicochem. Eng. Asp. 599 (2020), 124881, https://doi.org/10.1016/j.colsurfa.2020.124881.
[27] A. Gupta, M.M. Singh, Inhibition of mild steel corrosion in formic acid thiourea, 2-amino[4-p-choro phenyl] thiazole and different derivatives of their condensation products, Port. Electrochim. Acta. 17 (1999) 21–43, https://doi.org/10.4152/pea.199901021.
[28] Y. Ye, D. Yang, H. Chen, S. Guo, Q. Yang, L. Chen, H. Zhao, L. Wang, A high-efficiency corrosion inhibitor of N-doped citric acid-based carbon dots for mild steel in hydrochloric acid environment, J. Hazard. Mater. 381 (2020), 121019, https://doi.org/10.1016/j.jhazmat.2019.121019.
[29] P. Udhayakala, T.V. Rajendiran, S. Gunasekaran, Quantum chemical investigations on some quinoxaline derivatives as effective corrosion inhibitors for mild steel, Der Pharm. Lett. 4 (2012) 1285–1298.
[30] M. Galai, M. Rbaa, M. Ouakki, A.S. Abousalem, E. Ech-chihbi, K. Dahmani, N. Dkhireche, B. Lakhrissi, M. EbnTouhami, Chemically functionalized of 8-hydroxyquinoline derivatives as efficient corrosion inhibition for steel in 1.0M HCl solution: experimental and theoretical studies, Surf. Interfaces 21 (2020), 100695, https://doi.org/10.1016/j.surfin.2020.100695.
[31] R.T. Loto, Pyrimidine derivatives as environmentally-friendly corrosion inhibitors: a review, Int. J. Phys. Sci. 7 (2012) 2697–2705, https://doi.org/10.5897/ijps11.1579.
[32] K. Karrouchi, S. Radi, Y. Ramli, J. Taoufik, Y.N. Mabkhot, F.A. Al-Aizari, M. Ansar, Synthesis and pharmacological activities of Pyrazole derivatives: a review, 2018. https://doi.org/10.3390/molecules23010134.
[33] F.E.L Hajjaji, R. Salim, M. Taleb, F. Benhiba, N. Rezki, D.S. Chauhan, M. A. Quraishi, Pyridinium-based ionic liquids as novel eco-friendly corrosion inhibitors for mild steel in molar hydrochloric acid: experimental & computational approach, Surf. Interfaces 22 (2021), 100881, https://doi.org/10.1016/j.surfin.2020.100881.
[34] N.V. Likhanova, M.A. Domínguez-Aguilar, O. Olivares-Xometl, N. Nava-Entzana, E. Arce, H. Dorantes, The effect of ionic liquids with imidazolium and pyridinium cations on the corrosion inhibition of mild steel in acidic environment, Corros. Sci. 52 (2010) 2088–2097, https://doi.org/10.1016/j.corsci.2010.02.030.
[35] C. Verma, L.O. Olasunkanmi, I.B. Obot, E.E. Ebenso, M.A. Quraishi, 2,4-diamino-5-(phenylthio)-5: h -chromeno [2,3- b] pyridine-3-carbonitriles as green and effective corrosion inhibitors: gravimetric, electrochemical, surface morphology and theoretical studies, RSC Adv. 6 (2016) 53933–53948, https://doi.org/10.1039/c6ra04900a.
[36] R. Kumar, J. Arora, S. Ruhil, N. Phougat, A.K. Chhillar, A.K. Prasad, Synthesis and antimicrobial studies of pyrimidine pyrazole heterocycles, Adv. Chem. 2014 (2014) 1–12, https://doi.org/10.1155/2014/329681.
[37] B.M. Praveen, B.M. Prasanna, N. Hebbar, P.S. Kumar, M.R. Jagadeesh, Experimental and theoretical studies on inhibition effect of the praziquantel on mild steel corrosion in 1M HCl, J. Bio- Tribo-Corrosion. 4 (2018), https://doi.org/10.1007/s40735-018-0137-0.
[38] C.A.J. Richards, H.N. McMurray, G. Williams, Smart-release inhibition of corrosion driven organic coating failure on zinc by cationic benzotriazole based pigments, Corros. Sci. 154 (2019) 101–110, https://doi.org/10.1016/j.corsci.2019.04.005.
[39] C. Verma, M.A. Quraishi, K. Kluza, M. Makowska-Janusik, L.O. Olasunkanmi, E. E. Ebenso, Corrosion inhibition of mild steel in 1M HCl by D-glucose derivatives of dihydropyrido [2,3-d:6,5-d′] dipyrimidine-2, 4, 6, 8(1H,3H, 5H,7H)-tetraone, Sci. Rep. 7 (2017) 1–17, https://doi.org/10.1038/srep44432.
[40] B.S. Hou, Q.H. Zhang, Y.Y. Li, G.Y. Zhu, H.F. Liu, G.A. Zhang, A pyrimidine derivative as a high efficiency inhibitor for the corrosion of carbon steel in oilfield produced water under supercritical CO_2 conditions, Corros. Sci. (2020) 164, https://doi.org/10.1016/j.corsci.2019.108334.
[41] T.K. Sarkar, V. Saraswat, R.K. Mitra, I.B. Obot, M. Yadav, Mitigation of corrosion in petroleum oil well/tubing steel using pyrimidines as efficient corrosion inhibitor: experimental and theoretical investigation, Mater. Today Commun. (2020), 101862, https://doi.org/10.1016/j.mtcomm.2020.101862.
[42] B.A. Umar, A. Uzairu, G.A. Shallangwa, Understanding inhibition of steel corrosion by some potent triazole derivatives of pyrimidine through density functional theory and molecular dynamics simulation studies, J. Turkish Chem. Soc. Sect. A Chem. 6 (2019) 451–462, https://doi.org/10.18596/jotcsa.446084.
[43] M.M. Ibrahim, G.A.M. Mersal, A.M. Fallatah, M. Saracoglu, F. Kandemirli, S. Alharthi, S. Szunerits, R. Boukherroub, J. Ryl, M.A. Amin, Electrochemical, theoretical and surface physicochemical studies of the alkaline copper corrosion inhibition by newly synthesized molecular complexes of benzenediamine and tetraamine with π acceptor, J. Mol. Liq. 320 (2020), 114386, https://doi.org/10.1016/j.molliq.2020.114386.
[44] M. Yadav, S. Kumar, R.R. Sinha, I. Bahadur, E.E. Ebenso, New pyrimidine derivatives as efficient organic inhibitors on mild steel corrosion in acidic medium: electrochemical, SEM, EDX, AFM and DFT studies, J. Mol. Liq. 211 (2015) 135–145, https://doi.org/10.1016/j.molliq.2015.06.063.
[45] J. Haque, K.R. Ansari, V. Srivastava, M.A. Quraishi, I.B. Obot, Pyrimidine derivatives as novel acidizing corrosion inhibitors for N80 steel useful for petroleum industry: a combined experimental and theoretical approach, J. Ind. Eng. Chem. 49 (2017) 176–188, https://doi.org/10.1016/j.jiec.2017.01.025.
[46] M. Saracoglu, Z. Kokbudak, E. Yalcin, F. Kandemirli, Synthesis and DFT quantum chemical calculations of 2-oxopyrimidin-1(2H)-yl-urea and thiorea derivatives, J. Chem. Soc. Pak. 41 (2019) 841–858.
[47] Y. Gonzalez, M.C. Lafont, N. Pebere, G. Chatainier, J. Roy, T. Bouissou, A corrosion inhibition study of a carbon steel in neutral chloride solutions by zinc salt/phosphonic acid association, Corros. Sci. 37 (1995) 1823–1837, https://doi.org/10.1016/0010-938X(95)00085-X.
[48] Y. Valadbeigi, Proton affinities of hydrated molecules, Chem. Phys. Lett. 660 (2016) 301–306, https://doi.org/10.1016/j.cplett.2016.08.035.
[49] L. Guo, J. Tan, S. Kaya, S. Leng, Q. Li, F. Zhang, Multidimensional insights into the corrosion inhibition of 3,3-dithiodipropionic acid on Q235 steel in H2SO4 medium: a combined experimental and in silico investigation, J. Colloid Interface Sci. 570 (2020) 116–124, https://doi.org/10.1016/j.jcis.2020.03.001.
[50] B. El Ibrahimi, L. Bazzi, S. El Issami, The role of pH in corrosion inhibition of tin using the proline amino acid: theoretical and experimental investigations, RSC Adv. 10 (2020) 29696–29704, https://doi.org/10.1039/d0ra04333h.
[51] B. El Ibrahimi, Atomic-scale investigation onto the inhibition process of three 1,5-benzodiazepin-2-one derivatives against iron corrosion in acidic environment, Colloids Interface Sci. Commun. 37 (2020), 100279, https://doi.org/10.1016/j.colcom.2020.100279.
[52] R. Oukhrib, B. El Ibrahimi, H. Abou Oualid, Y. Abdellaoui, S. El Issami, L. Bazzi, M. Hilali, H. Bourzi, In silico investigations of alginate biopolymer on the Fe (110), Cu (111), Al (111) and Sn (001) surfaces in acidic media: quantum chemical and molecular mechanic calculations, J. Mol. Liq. 312 (2020), 113479, https://doi.org/10.1016/j.molliq.2020.113479.
[53] M.A. Migahed, A.A. Farag, S.M. Elsaed, R. Kamal, M. Mostfa, H.A. El-Bary, Synthesis of a new family of Schiff base nonionic surfactants and evaluation of their corrosion inhibition effect on X-65 type tubing steel in deep oil wells formation water, Mater. Chem. Phys. 125 (2011) 125–135, https://doi.org/10.1016/j.matchemphys.2010.08.082.
[54] M. Ghazi, Mothana G.K. Alfalah, F. Kandemirli, Corrosion inhibition potential of dithiohydrazodicarbonamide derivatives for mild steel in acid media : synthesis, experimental, DFT, and Monte Carlo studies, Arab. J. Sci. Eng. (2021), https://doi.org/10.1007/s13369-021-06368-y.
[55] H. Zhu, X. Chen, X. Li, J. Wang, Z. Hu, X. Ma, 2-aminobenzimidazole derivative with surface activity as corrosion inhibitor of carbon steel in HCl: experimental and theoretical study, J. Mol. Liq. 297 (2020), 111720, https://doi.org/10.1016/j.molliq.2019.111720.
[56] I. Ichchou, L. Larabi, H. Rouabhi, Y. Harek, A. Fellah, Electrochemical evaluation and DFT calculations of aromatic sulfonohydrazides as corrosion inhibitors for XC38 carbon steel in acidic media, J. Mol. Struct. (2019) 1198, https://doi.org/10.1016/j.molstruc.2019.126898.
[57] K. Cherrak, M.E. Belghiti, A. Berrissoul, M. El Massaoudi, M. El Faydy, M. Taleb, S. Radi, A. Zarrouk, A. Dafali, Pyrazole carbohydrazide as corrosion inhibitor for mild steel in HCl medium: experimental and theoretical investigations, Surf. Interfaces 20 (2020), 100578, https://doi.org/10.1016/j.surfin.2020.100578.

[58] R.G.M. de A. Macedo, N. do N. Marques, J. Tonholo, R. de C. Balaban, Water-soluble carboxymethylchitosan used as corrosion inhibitor for carbon steel in saline medium, Carbohydr. Polym. 205 (2019) 371–376, https://doi.org/10.1016/j.carbpol.2018.10.081.
[59] Ž.Z. Tasić, M.B. Petrović Mihajlović, M.B. Radovanović, A.T. Simonović, M. M. Antonijević, Cephradine as corrosion inhibitor for copper in 0.9% NaCl solution, J. Mol. Struct. 1159 (2018) 46–54, https://doi.org/10.1016/j.molstruc.2018.01.031.
[60] N. Errahmany, M. Rbaa, A.S. Abousalem, A. Tazouti, M. Galai, E.H. El Kafssaoui, M.E. Touhami, B. Lakhrissi, R. Touir, Experimental, DFT calculations and MC simulations concept of novel quinazolinone derivatives as corrosion inhibitor for mild steel in 1.0 M HCl medium, J. Mol. Liq. 312 (2020), 113413, https://doi.org/10.1016/j.molliq.2020.113413.
[61] M.G.K. AlFalah, E. Kamberli, A.H. Abbar, F. Kandemirli, M. Saracoglu, Corrosion performance of electrospinning nanofiber ZnO-NiO-CuO/polycaprolactone coated on mild steel in acid solution, Surf. Interfaces 21 (2020), 100760, https://doi.org/10.1016/j.surfin.2020.100760.
[62] M. Mobin, M. Basik, J. Aslam, Pineapple stem extract (Bromelain) as an environmental friendly novel corrosion inhibitor for low carbon steel in 1 M HCl, Meas. J. Int. Meas. Confed. 134 (2019) 595–605, https://doi.org/10.1016/j.measurement.2018.11.003.
[63] G. Sılircik, T. Tüken, M. Erbil, Inhibition efficiency of aminobenzonitrile compounds on steel surface, Appl. Surf. Sci. 324 (2015) 232–239, https://doi.org/10.1016/j.apsusc.2014.09.206.
[64] M. Rbaa, F. Benhiba, P. Dohare, L. Lakhrissi, R. Touir, B. Lakhrissi, A. Zarrouk, Y. Lakhrissi, Synthesis of new epoxy glucose derivatives as a non-toxic corrosion inhibitors for carbon steel in molar HCl: experimental, DFT and MD simulation, Chem. Data Collect. (2020) 27, https://doi.org/10.1016/j.cdc.2020.100394.
[65] M. Rbaa, M. Fardioui, C. Verma, A.S. Abousalem, M. Galai, E.E. Ebenso, T. Guedira, B. Lakhrissi, I. Warad, A. Zarrouk, 8-Hydroxyquinoline based chitosan derived carbohydrate polymer as biodegradable and sustainable acid corrosion inhibitor for mild steel: experimental and computational analyses, Int. J. Biol. Macromol. 155 (2020) 645–655, https://doi.org/10.1016/j.ijbiomac.2020.03.200.
[66] J. Yang, Y. Lu, Z. Guo, J. Gu, C. Gu, Corrosion behaviour of a quenched and partitioned medium carbon steel in 3.5wt.% NaCl solution, Corros. Sci. 130 (2018) 64–75, https://doi.org/10.1016/j.corsci.2017.10.027.
[67] M. Rbaa, F. Benhiba, A.S. Abousalem, M. Galai, Z. Rouifi, H. Oudda, B. Lakhrissi, I. Warad, A. Zarrouk, Sample synthesis, characterization, experimental and theoretical study of the inhibitory power of new 8-hydroxyquinoline derivatives for mild steel in 1.0M HCl, J. Mol. Struct. (2020) 1213, https://doi.org/10.1016/j.molstruc.2020.128155.
[68] M.A. Amin, S.S. Abd El-Rehim, E.E.F. El-Sherbini, R.S. Bayoumi, The inhibition of low carbon steel corrosion in hydrochloric acid solutions by succinic acid. Part I. Weight loss, polarization, EIS, PZC, EDX and SEM studies, Electrochim. Acta. 52 (2007) 3588–3600, https://doi.org/10.1016/j.electacta.2006.10.019.
[69] M. Chafiq, A. Chaouiki, H. Lgaz, R. Salghi, K.V. Bhaskar, R. Marzouki, K.S. Bhat, I. H. Ali, M.I. Khan, I.M. Chung, Inhibition performances of spirocyclopropane derivatives for mild steel protection in HCl, Mater. Chem. Phys. 243 (2020), 122582, https://doi.org/10.1016/j.matchemphys.2019.122582.
[70] Z. Zhang, S. Chen, Y. Li, S. Li, L. Wang, A study of the inhibition of iron corrosion by imidazole and its derivatives self-assembled films, Corros. Sci. 51 (2009) 291–300, https://doi.org/10.1016/j.corsci.2008.10.040.
[71] M. El Faydy, B. Lakhrissi, A. Guenbour, S. Kaya, F. Bentiss, I. Warad, A. Zarrouk, In situ synthesis, electrochemical, surface morphological, UV–visible, DFT and Monte Carlo simulations of novel 5-substituted-8-hydroxyquinoline for corrosion protection of carbon steel in a hydrochloric acid solution, J. Mol. Liq. 280 (2019) 341–359, https://doi.org/10.1016/j.molliq.2019.01.105.
[72] A.A. Farag, A.S. Ismail, M.A. Migahed, Environmental-friendly shrimp waste protein corrosion inhibitor for carbon steel in 1 M HCl solution, Egypt. J. Pet. 27 (2018) 1187–1194, https://doi.org/10.1016/j.ejpe.2018.05.001.
[73] D.S. Chauhan, K.R. Ansari, A.A. Sorour, M.A. Quraishi, H. Lgaz, R. Salghi, Thiosemicarbazide and thiocarbohydrazide functionalized chitosan as ecofriendly corrosion inhibitors for carbon steel in hydrochloric acid solution, Int. J. Biol. Macromol. 107 (2018) 1747–1757, https://doi.org/10.1016/j.ijbiomac.2017.10.050.
[74] M. Parveen, M. Mobin, S. Zehra, R. Aslam, L-proline mixed with sodium benzoate as sustainable inhibitor for mild steel corrosion in 1M HCl: an experimental and theoretical approach, Sci. Rep. 8 (2018) 1–18, https://doi.org/10.1038/s41598-018-24143-2.
[75] I. Selatnia, A. Sid, M. Benahmed, O. Dammene debbih, T. Ozturk, N. Gherraf, Synthesis and characterization of a bis-pyrazoline derivative as corrosion inhibitor for A283 carbon steel in 1M HCl: electrochemical, surface, DFT and MD simulation studies, Prot. Met. Phys. Chem. Surfaces. 54 (2018) 1182–1193, https://doi.org/10.1134/S2070205118060229.
[76] Y. Ma, F. Han, Z. Li, C. Xia, Acidic-functionalized ionic liquid as corrosion inhibitor for 304 stainless steel in aqueous sulfuric acid, ACS Sustain. Chem. Eng. 4 (2016) 5046–5050, https://doi.org/10.1021/acssuschemeng.6b01492.
[77] J. Tan, L. Guo, H. Yang, F. Zhang, Y. El Bakri, Synergistic effect of potassium iodide and sodium dodecyl sulfonate on the corrosion inhibition of carbon steel in HCl medium: a combined experimental and theoretical investigation, RSC Adv 10 (2020) 15163–15170, https://doi.org/10.1039/d0ra02011g.
[78] H. El Aadad, M. Galai, M. Ouakki, A. Elgendy, M.E. Touhami, A. Chahine, Improvement of the corrosion resistance of mild steel in sulfuric acid by new organic-inorganic hybrids of benzimidazole-pyrophosphate: facile synthesis, characterization, experimental and theoretical calculations (DFT and MC), Surf. Interfaces 24 (2021), 101084, https://doi.org/10.1016/j.surfin.2021.101084.
[79] P.K. Paul, M. Yadav, I.B. Obot, Investigation on corrosion protection behavior and adsorption of carbohydrazide-pyrazole compounds on mild steel in 15% HCl solution: electrochemical and computational approach, J. Mol. Liq. 314 (2020), 113513, https://doi.org/10.1016/j.molliq.2020.113513.
[80] A.S. Sowmyashree, A. Somya, C.B.P. Kumar, S. Rao, Novel nano corrosion inhibitor, integrated zinc titanate nano particles: synthesis, characterization, thermodynamic and electrochemical studies, Surf. Interfaces 22 (2020), 100812, https://doi.org/10.1016/j.surfin.2020.100812.
[81] X. Zhou, H. Yang, F. Wang, BF4 ionic liquids as effective inhibitor for carbon steel in alkaline chloride solution, Electrochim. Acta. 56 (2011) 4268–4275, https://doi.org/10.1016/j.electacta.2011.01.081.
[82] G.Y. Elewady, Pyrimidine derivatives as corrosion inhibitors for carbon-steel in 2M hydrochloric acid solution, Int. J. Electrochem. Sci. 3 (2008) 1149–1161.
[83] S. Lahmidi, A. Elyoussfi, A. Dafali, H. Elmsellem, N.K. Sebbar, L. El Ouasif, A. E. Jilalat, B. El Mahi, E.M. Essassi, I. Abdel-Rahman, B. Hammouti, Corrosion inhibition of mild steel by two new 1,2,4-triazolo[1,5-a] pyrimidine derivatives in 1M HCl: experimental and computational study, J. Mater. Environ. Sci. 8 (2017) 225–237.